fibers

MDPI

Article

Performance Prediction of GFRP-Reinforced Concrete Deep Beams Containing a Web Opening in the Shear Span

Amena Sheikh-Sobeh, Nancy Kachouh and Tamer El-Maaddawy *

Department of Civil and Environmental Engineering, College of Engineering, Al Ain Campus, United Arab Emirates University, Al Ain P.O. Box 15551, United Arab Emirates; 202070414@uaeu.ac.ae (A.S.-S.); 201890034@uaeu.ac.ae (N.K.)

* Correspondence: tamer.maaddawy@uaeu.ac.ae

Abstract: This study aimed to investigate the nonlinear structural behavior of concrete deep beams internally reinforced with glass fiber-reinforced polymer (GFRP) reinforcing bars and containing a web opening of various sizes and locations within the shear span. Three-dimensional (3D) numerical simulation models were developed for large-scale GFRP-reinforced concrete deep beams (300 mm × 1200 mm × 5000 mm) with a shear span-to-depth ratio (a/h) of 1.04. Predictions of the numerical models were validated against published experimental data. A parametric study was conducted to examine the effect of varying the opening size and location on the shear response. Results of the numerical analysis indicated that the strength of the deep beam models with an opening in the middle of the shear span decreased with an increase in either the opening width or height. The rate of the strength reduction caused by increasing the opening height was, however, more significant than that produced by increasing the opening width. Placing a web opening in the compression zone close to the load plate was very detrimental to the beam strength. Conversely, a negligible strength reduction was recorded when the web opening was placed in the tension side above the flexural reinforcement and away from the natural load path. Data of the parametric study were utilized to introduce simplified analytical formulas capable of predicting the shear capacity of GFRP-reinforced concrete deep beams with a web opening in the shear span.

Keywords: deep beams; GFRP; numerical; openings; simulation; shear

Citation: Sheikh-Sobeh, A.; Kachouh, N.; El-Maaddawy, T. Performance Prediction of GFRP-Reinforced Concrete Deep Beams Containing a Web Opening in the Shear Span. *Fibers* **2024**, *12*, 66. https://doi.org/10.3390/fib12080066

Academic Editor: Luciano Ombres

Received: 6 May 2024
Revised: 23 July 2024
Accepted: 29 July 2024
Published: 6 August 2024

1. Introduction

Discontinuity regions (D-regions) are formed in reinforced concrete (RC) beams due to statical or geometric discontinuities [1,2]. The former are regions near concentrated loads and support reactions, whereas the latter are regions adjacent to web openings or abrupt changes in cross-section [1,2]. Concrete deep beams, i.e., a shear span-to-depth ratio (a/h) ≤ 2, with and without cutouts, are influenced by both statical and geometric discontinuities [1,2]. The discontinuity in statical loading or geometry causes a complex flow of internal stresses and nonlinear distribution of longitudinal strains within the cross-section. As such, the traditional beam theory (Bernoulli hypothesis) applied in the analysis of conventional RC structural members (B-regions), is not valid for the analysis of D-regions [1,2]. Traditionally, D-regions in structural concrete members reinforced with steel reinforcing bars have been designed using dissimilar empirical equations that are not universally applicable [3,4]. The problem becomes more challenging when conventional steel reinforcing bars are replaced by nonmetallic reinforcement such as fiber-reinforced polymer (FRP) composites.

Nonmetallic fiber-reinforced polymer (FRP) reinforcing bars, including basalt FRP (BFRP), carbon FRP (CFRP), and glass FRP (GFRP), are considered a viable prospective alternative to conventional steel reinforcement because of their high strength, light weight, and noncorrosive nature [5–10]. Specific types of composite reinforcement, such as GFRP

bars, are also nonconductive and nonmagnetic. As such, corrosion problems and magnetic interference can be eliminated through the use of FRP reinforcing bars in concrete structures [5–10]. Because of their numerous advantages, research on the shear behavior of concrete deep beams internally reinforced with FRP bars has attracted several researchers over the last two decades [11–24]. On the other hand, FRP bars possess different mechanical properties than those of steel bars, such as a linear stress–strain relationship until failure and lower modulus of elasticity, that make the design provisions for steel-reinforced deep beams not directly applicable to FRP-reinforced deep beams [25,26]. The proper design of FRP-reinforced elements is crucial, which calls for investigating the arch action developed by FRP-reinforced deep beams.

The load-deflection response of FRP-reinforced deep beams is typically bilinear [11–22]. This behavior is comparable to that reported for steel-reinforced deep beams [27–29]. GFRP-reinforced deep beams typically fail in a brittle manner because of the crushing in the diagonal compression strut, which is consistent with the failure mode of steel-reinforced deep beams [21,22,27]. Deep beams reinforced with BFRP/GFRP reinforcing bars exhibited a greater midspan deflection and a lower shear capacity relative to those of their steel-reinforced counterparts due to the lower elastic modulus, lower transverse strength, and lower dowel action of the BFRP/GFRP reinforcing bars [12,22,25]. Increasing the section height reduced the normalized shear stress at ultimate load of BFRP/GFRP-reinforced deep beams [14,22]. The reduction in the normalized shear stress at ultimate load of BFRP-reinforced deep beams due to an increase in the section size was greater than that of their steel-reinforced counterparts [20,22]. The bond performance of embedded FRP rebars in concrete was inferior to that of steel rebars [26]. The bond quality of FRP rebars can be enhanced by using high-strength concrete materials to improve the load-bearing resistance of structural members such as RC deep beams [26].

Numerous studies have examined the shear behavior of FRP-reinforced concrete deep beams without web reinforcement [11–20]. The shear capacity of solid deep beams reinforced with FRP bars improved with an increase in the value of a/h, the reinforcement ratio/modulus of elasticity of longitudinal FRP bars, and concrete compressive strength [11–20]. An inverse linear correlation between the shear capacity and the cubic root of a/d was reported for solid deep beams reinforced with BFRP bars, where d is the beam effective depth [17,18]. The increase in the shear capacity of FRP-reinforced deep beams due to decreasing a/h can be ascribed to an increase in the angle of inclination and/or width of the inclined concrete strut that governed the beam failure [15]. Increasing the GFRP reinforcement ratio in concrete deep beams controlled the widening of shear cracks, and hence increased the shear strength [12,13]. The enhancement in the shear strength of GFRP-reinforced concrete deep beams due to an increase in the concrete compressive strength may have a threshold, after which a minor additional increase in the shear capacity may be recorded [12]. It is noteworthy that a significant increase in the longitudinal reinforcement ratio together with the concrete strength could be detrimental to the shear strength of GFRP-reinforced short beams without web reinforcement due to a change in the mode of failure from strut crushing to diagonal splitting [19].

Little information is available in the literature on the shear behavior of FRP-reinforced deep beams with web reinforcement and/or cutouts [21–24]. The use of vertical GFRP stirrups improved the shear capacity of solid GFRP-reinforced large-scale deep beams by 20%, whereas the use of horizontal web reinforcement solely was detrimental to the shear strength because of the high tensile strains in the horizontal bars that induced deterioration and softening of the concrete in the diagonal strut [21]. An increase in the value of a/h for deep beams with BFRP web reinforcement reduced the normalized ultimate shear strength but had an ignorable influence on the size effect [22]. The presence of a web opening, with an opening width-to-shear span ratio of w_o/a = 0.27 and an opening height-to-beam depth ratio of h_o/h = 0.25, in the middle of the shear span of a large-scale GFRP-reinforced deep beam, with a/h = 1 and minimum shear reinforcement, reduced the shear capacity by 54%, relative to that of its solid counterpart [23]. Providing additional GFRP shear reinforcement

around the web opening increased the shear capacity by 20–56% compared to that of the deep beam without additional reinforcement around the openings [23]. The use of diagonal GFRP reinforcement in the upper and lower chords of concrete deep beams with a web opening improved the shear capacity [24]. Placing the diagonal GFRP reinforcement in the lower chord rather than in the upper chord was more effective in improving the shear capacity of GFRP-reinforced deep beams with a web opening [24]. Despite the interesting findings and useful information offered in the aforementioned study [24], the beams did not include minimum GFRP shear reinforcement, which is impractical and not in compliance with the requirements of international design guides and standards (e.g., CSA S806 [5] and ACI 440.1R [6]).

Previous studies highlighted the lack of knowledge on the shear behavior of GFRP-reinforced concrete deep beams with a web opening in the shear span [30]. The interaction between the opening size and opening location in GFRP-reinforced deep beams was not investigated. This study aims to fill this gap through numerical analysis. Three-dimensional (3D) simulation models capable of predicting the structural shear behavior of GFRP-reinforced concrete beams with D-regions were developed using ATENA® software (v. 5.9.0k) [31] and validated against experimental data from [23]. A parametric study was conducted to investigate the effect of key parameters on the shear response of GFRP-reinforced deep beams. Refined analytical formulas were then developed to assist practitioners in predicting the shear capacity of GFRP-reinforced deep beams with a web opening.

The findings of the present study are anticipated to assist practitioners and researchers in designing concrete D-regions reinforced with GFRP bars. The outcomes of the study are anticipated to advance the development of design guidelines and standards on reinforcing concrete structures with GFRP bars. The widespread use of GFRP reinforcing bars instead of the conventional steel reinforcement in construction would reduce repair cycles and operational costs, thus leading to long-lasting sustainable structures.

2. Model Development

2.1. Geometry of the Beam Models

Details of the reinforcement of the deep beam models used for verification against the experimental data from [23], DB-S, DB-O1, DB-O2, and DB-O3, are shown in Figure 1a–d, respectively. The deep beam models were 5000 mm long, 300 mm wide, and 1200 mm deep. The effective span of the beams was 3000 mm, the shear span was 1250 mm, and the shear span-to-depth ratio (a/h) was 1.04. One deep beam model was solid (DB-S), whereas the other three models (DB-O1, DB-O2, and DB-O3) had a web opening in the middle of the shear span with a width (w_o) of 340 mm and height (h_o) of 304 mm, which corresponded to an opening width-to-shear span ratio (w_o/a) of 0.27 and an opening height-to-beam depth ratio (h_o/h) of 0.25. Figure 1a shows the location of monitoring points on the GFRP reinforcing bars of the solid deep beam model, whereas Figure 1b shows the location of monitoring points on the GFRP reinforcing bars of a deep beam model with an opening. For clarity purposes the monitoring points are not shown in Figure 1c,d. The longitudinal reinforcement in the tension side consisted of eight GFRP bars with a diameter of 25 mm (No. 25) placed at a distance d = 1100 mm from the compression face. The compression reinforcement consisted of two GFRP bars with a diameter of 16 mm (No. 16). The internal shear reinforcement consisted of vertical and horizontal GFRP bars with diameters of 12 mm (No. 12) and 16 mm (No. 16), respectively, placed at a spacing of 200 mm in both directions. The deep beam model DB-O2 had 2 extra double-leg GFRP stirrups in the vertical direction (one at each side of the opening), 2 extra horizontal GFRP bars above the opening, and 2 extra horizontal GFRP bars below the opening. The deep beam model DB-O3 had 4 extra double-leg GFRP stirrups in the vertical direction (one at each side of the opening and two crossed by the opening), 4 extra horizontal GFRP bars above the opening, and 4 extra horizontal GFRP bars below the opening. All the extra GFRP reinforcing bars

in deep beam models DB-O2 and DB-O3 had a diameter of 12 mm (No. 12). Steel plates (200 mm × 300 mm × 30 mm) were placed at the load and support points.

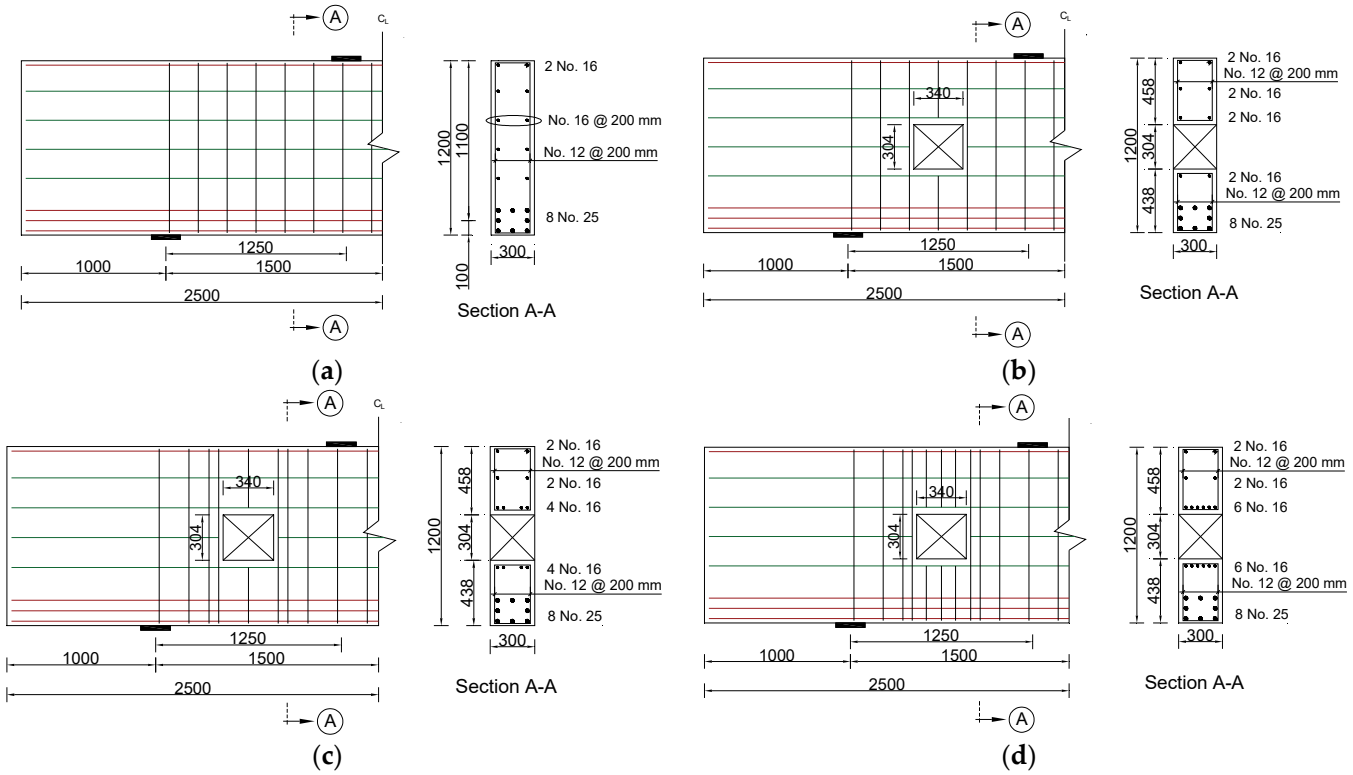

Figure 1. Details of the deep beam models, noting that bars with red, green, and black colors represent the main flexural reinforcement, the horizontal web reinforcement, and the vertical web reinforcement, respectively (dimensions are in mm): (**a**) DB-S; (**b**) DB-O1; (**c**) DB-O2; (**d**) DB-O3.

2.2. Constitutive Laws of Materials

Figure 2a,b show the concrete compressive hardening and softening, respectively, whereas the tensile softening law is shown in Figure 2c. The uniaxial constitutive laws of concrete in compression and tension begin with a linear relationship, with a slope equal to the concrete modulus of elasticity (E_c). The compressive hardening phase starts at a stress value of $f'_{co} = 2.1f_t$, where f_t is the uniaxial tensile strength, and ends at a peak stress, f'_c and a corresponding plastic strain, ε_{cp}. The values of f_t and ε_{cp} are generated automatically by the software based on the concrete compressive strength [31]. The post peak compressive stress decreases linearly with an increase in the displacement (w_c) throughout the length scale (L_c). The value of w_c can be calculated at any plastic strain ε_p through the relationship $w_c = (\varepsilon_p - \varepsilon_{cp})L_c$. The default value of the displacement at zero stress (w_d) is 0.5 mm [31]. The tensile softening law decreases exponentially from the peak tensile stress, f_t, function of the crack opening displacement (w_t) that is calculated by the product of the fracturing strain (ε_{cf}) and the length scale (L_t) [31]. The crack opening at the complete release of stress (w_{tc}) is determined automatically by the software based on f_t and the specific fracture energy of the material (G_f). The cylindrical compressive strength (f_c') of the concrete was 37 MPa, except for DB-O3, which had an f_c' value of 45 MPa. Key input parameters of the concrete material used in the analysis are provided in Table 1.

The behavior of GFRP reinforcing bars was modeled as linear elastic until failure. The vertical GFRP stirrups having a diameter of 12 mm (No. 12) had a cross-sectional area of 127 mm^2, an elastic modulus of 50.0 GPa, and a tensile strength of 1019 MPa at the straight portion [23]. It is noteworthy that the tensile strength of the bent portions of the vertical stirrups (459 MPa) was 45% of that of straight portions (1019 MPa), as reported in Reference [23]. The strength reduction that typically occurs in the bent portions of FRP

bars is attributed to the bending of fibers and the stress concentration that happens at the beginning of the bent portion, inducing premature failure at this location [5,6,32,33]. As such, the vertical GFRP stirrups were divided into segments so that a reduced tensile strength can be assigned to the bent portions of the stirrups. The horizontal GFRP bars with a diameter of 16 mm (No. 16) had a cross-sectional area of 198 mm^2, a tensile strength of 1184 MPa, and an elastic modulus of 62.6 GPa [14]. The flexural GFRP bars in the tension side having a diameter of 25 mm (No. 25) had a cross-sectional area of 507 mm^2, a tensile strength of 1000 MPa, and an elastic modulus of 66.4 GPa [14]. A perfect bond was assumed between the GFRP reinforcing bars and the surrounding concrete. The validity of the perfect bond assumption between the GFRP bars and the concrete and its adequacy to produce a reasonable prediction for the load capacity of GFRP-reinforced concrete beams was reported in previous studies [34,35]. The comparative analysis between predictions of the numerical models developed in the present study and the corresponding published experimental data, presented in Section 3 of this manuscript, further verifies the validity of this assumption. The numerical models developed and verified in the present study can be used in future research to compare the behavior of GFRP-reinforced concrete beams with a web opening to other similar beams reinforced with conventional steel bars with various yielding strengths. It is noteworthy that the contribution of the GFRP reinforcing bars around the opening is mostly provided by the vertical stirrups around the opening and the continuous horizontal bars in the top and bottom chords located above and below the opening, respectively. The horizontal bars intercepted by the opening are stopped near the surface of the opening. In most cases, these bars are not intercepted by the critical shear crack causing failure. As such, the contribution of the horizontal bars cut by the opening to the shear resistance provided by the reinforcement may be considered not critical relative to that of other GFRP reinforcement crossed by the critical load path in the upper and bottom chords. Future research should further investigate the effect of the anchorage length and bond condition of the horizontal bars cut by the opening on the response of the GFRP-reinforced deep beams.

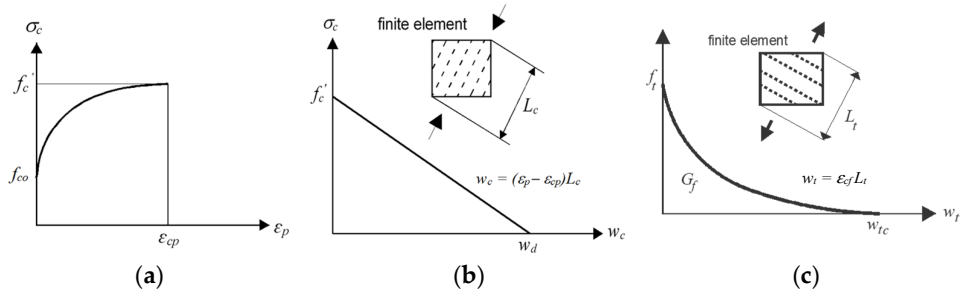

Figure 2. Constitutive laws of concrete: (**a**) compressive hardening; (**b**) compressive softening; (**c**) tensile softening.

Table 1. Key input parameters of the concrete.

Parameter	Description	Value *	Unit
f'_c	Compressive strength	37.00 (45.00)	MPa
E_c	Elastic modulus	33,254.00 (35,496.00)	MPa
μ	Poisson's ratio	0.2	N/A
f_t	Tensile strength	2.83 (3.33)	MPa
G_f	Specific fracture energy	70.75 (83.25)	N/m
ε_{cp}	Plastic concrete strain at compressive strength	0.0011 (0.0012)	N/A
w_d	Critical compressive displacement	0.50	mm

* Values between parenthesis are for DB-O3.

2.3. Types of Element and Boundary Conditions

Solid 3D macro-elements were used to model the concrete and steel plates. The GFRP bars were modeled as one-dimensional elements embedded into the macro-elements of the concrete. One half of the beam was modeled to optimize the processing time. A mesh sensitivity analysis was carried out to determine the optimum mesh size, which was found to be 50 mm. The support plate was restricted from movement in the transverse and vertical directions. Surface support was also used to prevent the surface at the plane of symmetry from moving in the direction normal to the other symmetrical part of the beam. The beams were subjected to two concentrated loads placed symmetrically around the midspan. Concentrated loads represent loads of columns planted on deep beams, which is commonly used in practical settings in ground and/or transfer floors of high-rise buildings. It is noteworthy that practical applications may also include deep beams loaded through a slab. In such a case, the beams are subjected to uniform loads. Deep beams with uniform loads may fail at a higher shear force than those of similar beams with concentrated loads [27]. The loading scheme adopted in the analysis was displacement-controlled at a prescribed displacement of 0.1 mm/step applied at the middle of the top surface of the loading plate. Monitoring points were used to measure the load and midspan deflection. The top and bottom steel plates were connected to the beam through fixed contacts. The standard Newton–Raphson iterative solution implemented in ATENA® software (v. 5.9.0k) was adopted [31]. Figure 3a shows a typical numerical model for a solid deep beam, while Figure 3b shows a typical numerical model for a beam with a web opening in the middle of the shear span. General 3D views showing the flexural and web reinforcements of the numerical models are provided in Figure 4.

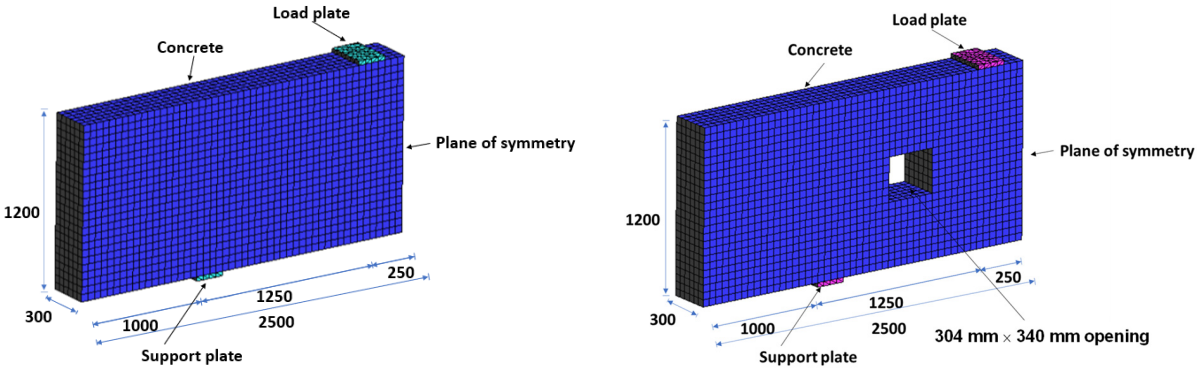

Figure 3. Numerical model (dimensions are in mm): (**a**) DB-S; (**b**) DB-O.

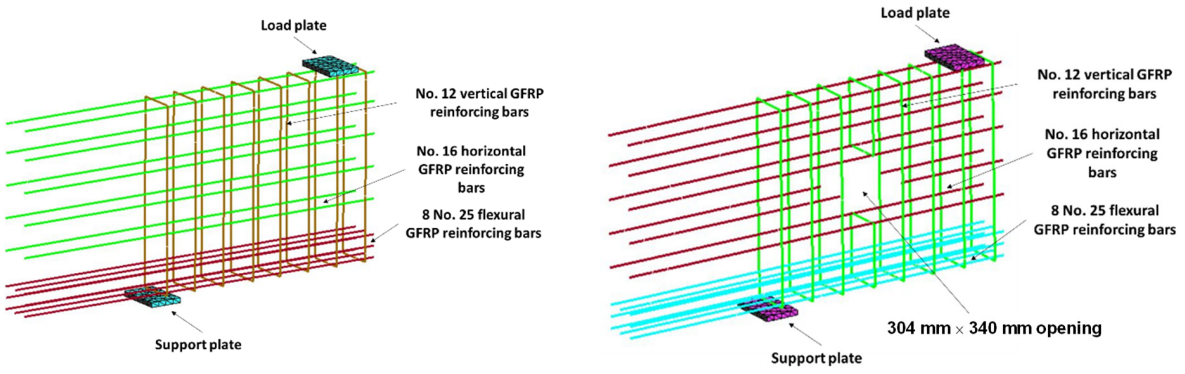

Figure 4. *Cont.*

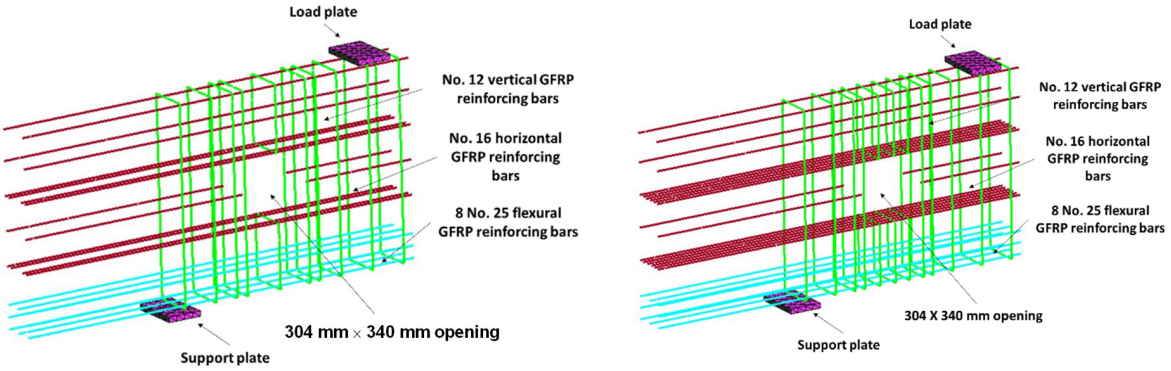

(**c**) (**d**)

Figure 4. Flexural and web reinforcements: (**a**) DB-S (Bars with red, green, and brown colors represent flexural tensile reinforcement, horizontal web reinforcement, and vertical web reinforcement, respectively); (**b**) DB-O1 (Bars with cyan, red, and green colors represent flexural tensile reinforcement, horizontal web reinforcement, and vertical web reinforcement, respectively); (**c**) DB-O2 (Bars with cyan, red, and green colors represent flexural tensile reinforcement, horizontal web reinforcement, and vertical web reinforcement, respectively); (**d**) DB-O3 (Bars with cyan, red, and green colors represent flexural tensile reinforcement, horizontal web reinforcement, and vertical web reinforcement, respectively).

3. Model Verification

The numerical models were verified against experimental data of four large-scale RC deep beams published in one of the top-tier journals [23]. One of these beams was solid (DB-S), whereas the other three beams (DB-O1, DB-O2, and DB-O3) had a web opening in the shear span with different amounts of GFRP reinforcement around the opening. Model verification against experimental data of such large-scale beams may be considered adequate given the scope and complexity of the topic. It is noteworthy that no studies on large-scale GFRP-reinforced deep beams with a web opening are currently available in the literature except for that used in the model verification of the present work. Future research should consider studying the effect of using different types of reinforcing bars (e.g., carbon, glass, steel with different yield strengths) on the behavior of concrete deep beams with a web opening in the shear span.

3.1. Load-Deflection Response

The numerically predicted responses of DB-S, DB-O1, DB-O2, and DB-O3 are compared to experimental data from [23] in Figure 5. The numerically predicted responses started with a linear branch until flexural cracks initiated at approximately 500 kN. There was a deviation between the pre-cracking stiffness predicted numerically and that measured experimentally. This behavior is expected, particularly for such a large-scale deep beam. The actual deep beams could have had shrinkage cracks due to the large surface area prior to testing, which might have reduced its initial stiffness in the pre-cracking stage. The initiation of the flexural cracks caused a change in the load-deflection response. The beam models exhibited a quasilinear response in the post-cracking phase due to a progressive development of cracks during loading, which was in alignment with the experimental results. The post-cracking stiffness of the deep beams with openings was lower than that of the solid beam. Another change in slope was observed prior to reaching the ultimate load in DB-S, probably because of the development of a new major crack and/or localized rupture at the bent portion of a vertical stirrup. It is noteworthy that the post-cracking stiffness of all beams predicted numerically almost coincided with that measured experimentally. Table 2 presents the numerical and experimental ultimate loads along with the corresponding deflection capacities. The difference between the numerical and experimental ultimate loads was within a 12% error band. The deviation between the deflection capacity predicted numerically and that obtained from the tests did not exceed 15%, except for DB-O3 which

showed a deviation of 28% in the deflection capacity. Generally, the difference between the numerical and experimental results is within the acceptable margin of error.

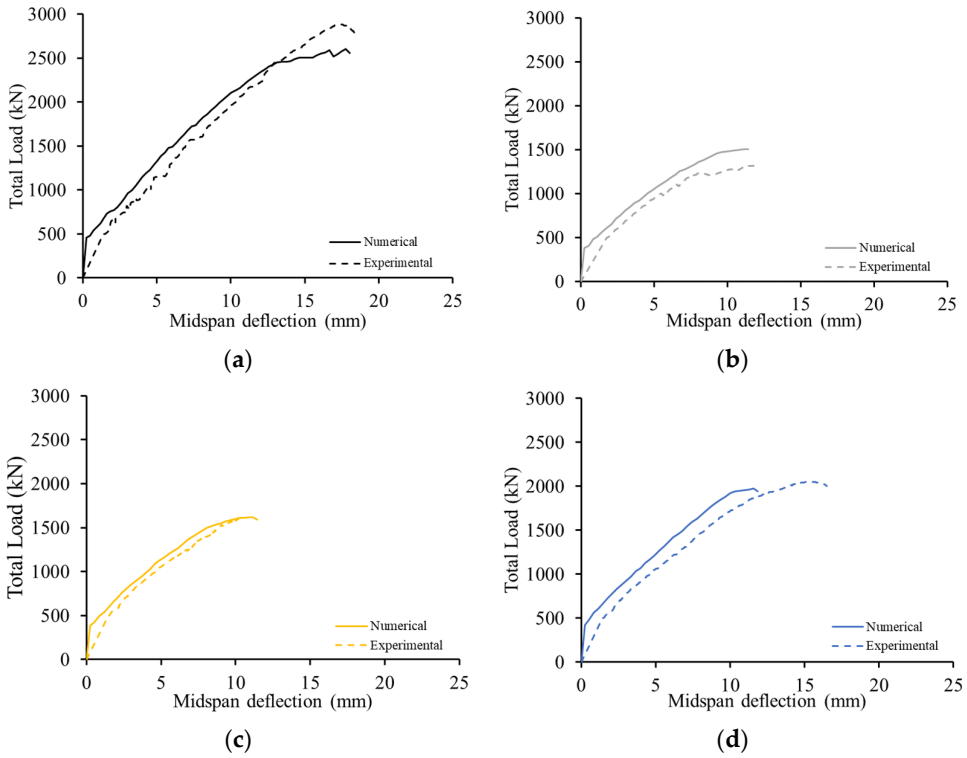

Figure 5. Load-deflection response predicted numerically vs. that obtained from the experiment based on data from [23]: (**a**) DB-S; (**b**) DB-O1; (**c**) DB-O2; (**d**) DB-O3.

Table 2. Numerical vs. experimental results.

Models	Ultimate Load (kN)			Deflection Capacity (mm)		
	Experimental [1]	Numerical	Error (%) [2]	Experimental [1]	Numerical	Error (%) [2]
DB-S	2904	2601	−10%	17.3	17.8	+3%
DB-O1	1328	1489	+12%	12.7	10.8	+15%
DB-O2	1619	1619	0%	11.3	11.2	−0.9%
DB-O3	2067	1978	−4%	16.2	11.6	−28%

[1] Experimental data from [23]; [2] Error $(\%) = \frac{\text{Numerical} - \text{Experimental}}{\text{Experimental}} \times 100$.

3.2. Crack Pattern and Failure Mode

The crack patterns predicted numerically at different stages of loading for DB-S are shown in Figure 6, whereas Figure 7 shows those for a typical deep beam model with a web opening (DB-O2). Schematics of the crack patterns obtained from the experiments based on data obtained from [23] for DB-S and a typical deep beam with a web opening are shown in Figure 8a,b respectively. From Figure 6, it can be seen that the numerical prediction of crack development for DB-S indicated the initiation of flexural cracks prior to shear cracks. The experimental data from [23] also indicated the initiation of flexural cracks early at 18% of the ultimate load before the development of any shear cracks. Diagonal cracks were then formed in the shear span as the load progressed. Additional shear cracks were developed with an increase in the applied load defining the direction of a concrete diagonal strut between the load and support points. Eventually, DB-S failed by crushing of the diagonal concrete strut formed in the shear span, which was in alignment with the mode of failure reported in the literature [23], as shown in Figure 8a.

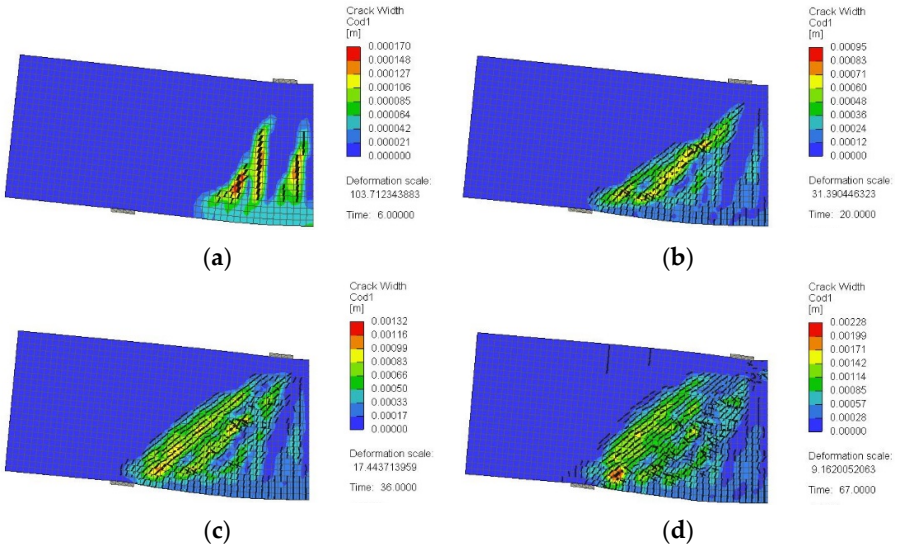

Figure 6. Numerical crack pattern of DB-S: (**a**) at 25% of peak load; (**b**) at 50% of peak load; (**c**) at 75% of peak load; (**d**) at 100% of peak load.

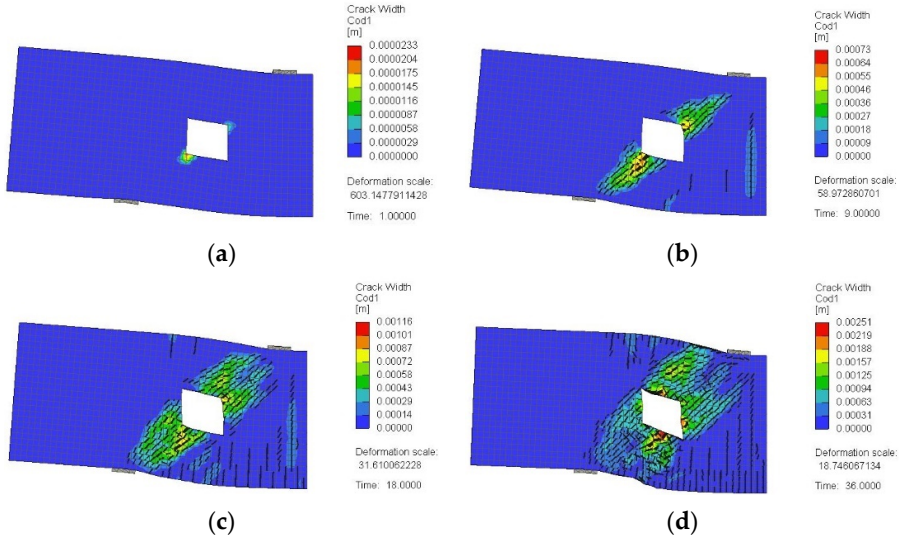

Figure 7. Crack pattern for a typical beam model with a web opening (DB-O2): (**a**) at 25% of peak load; (**b**) at 50% of peak load; (**c**) at 75% of peak load; (**d**) at 100% of peak load.

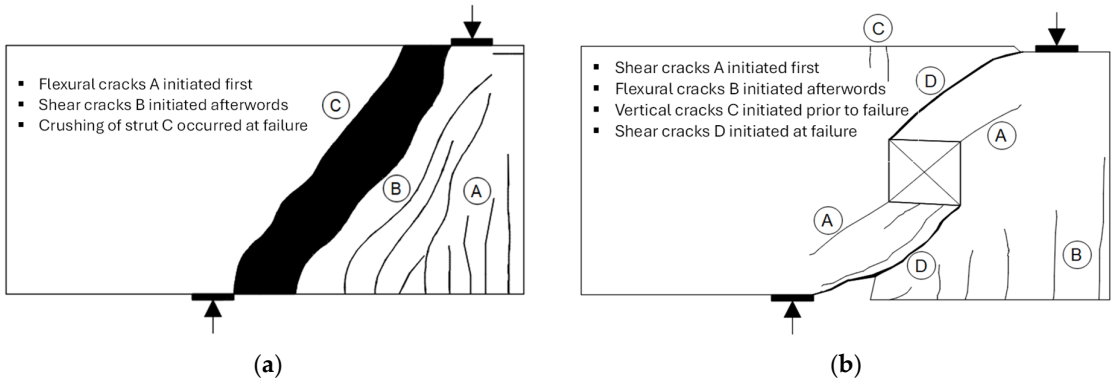

Figure 8. Schematics showing the crack patterns obtained from the experiments based on data from [23]: (**a**) solid beam; (**b**) beam with a web opening.

Figure 7 shows the crack patterns predicted numerically at different stages of loading for a typical deep beam model with a web opening (DB-O2). Shear cracks initiated first at the opposite corners of the opening closer to the support and load plates. This behavior was in agreement with the experimental data from [23], which indicated the early formation of shear cracks at the opening corner at 17 to 24% of the ultimate load. A further increase in load resulted in the development of flexural cracks and propagation of these shear cracks toward the load and support plates along with the development of flexural cracks. The shear cracks that developed earlier at the opening corners were then stabilized and other shear cracks then developed in the top and bottom chords. Eventually, the beam model with a web opening failed due to the formation of two independent major shear cracks that developed in the top and bottom chords. The major shear crack causing failure in the top chord connected the edge of the load plate to the top corner of the opening closer to the support plate. The major shear crack causing failure in the bottom chord connected the edge of the support plate and the bottom corner of the opening closer to the load point. The crack patterns at the different stages of loading and the failure mechanism predicted numerically were in good agreement with the sequence of crack propagation and failure mode observed during the experimental tests reported in the literature [23], as shown in Figure 8b.

3.3. GFRP Stresses

Figures 9–11 show the stresses in the vertical stirrups, horizontal web reinforcement, and flexural reinforcement of the deep beam models at peak load, respectively. Portions of the web GFRP reinforcement crossing the diagonal strut in DB-S exhibited the highest stresses, as shown in Figure 9a. The vertical concentrated load caused indirect tensile stresses in the top horizontal portion of the vertical stirrup under the load point in DB-S. The stress in this location was almost equal to that of the tensile strength of the bent portion of GFRP bars, indicating localized rupture of GFRP at this location. These numerical findings are consistent with the published experimental data [23], which indicated that crushing of the diagonal concrete strut in DB-S was accompanied by a localized rupture at the bent portion of the vertical stirrups. For DB-O1, the stress in the bent portions of the vertical GFRP stirrups at the sides of the opening almost reached the tensile strength of the bent portion of GFRP bars (Figure 9b). The experimental findings also indicated that rupture of the bent portions of the vertical GFRP stirrups near the load and support plates occurred at the ultimate load along with the crushing of concrete along the diagonal cracks that developed in the upper and lower chords [23]. In agreement with the published data [14], the predicted stresses in the vertical stirrups for DB-O2 and DB-O3, having extra GFRP reinforcement around the opening, were below the tensile strength of the bent portion of GFRP bars (Figure 9c). These results verify the effectiveness of the extra GFRP bars in relieving the web reinforcement, which allowed the beam models to develop a higher load capacity. The stresses in the horizontal web reinforcement in DB-O2 and DB-O3 at peak load were also lower than those of DB-O1 (Figure 10). From Figure 11, it can be seen that the maximum stress in the flexural reinforcement at peak load for DB-S was 390 MPa (i.e., 39% of the tensile strength of straight GFRP bars). The models with a web opening failed at a lower load than that of DB-S, and hence, the maximum stress in the flexural reinforcement was lower at an average value of 265 MPa (i.e., 27% of the tensile strength of straight GFRP bars). Published experimental data [23] verified the nonoccurrence of the rupture of the flexural GFRP reinforcement in the tested deep beams. It is noteworthy that the negative stress in the top GFRP longitudinal reinforcement in DB-S at ultimate load was higher than that of their counterparts with a web opening because DB-S failed at a higher load.

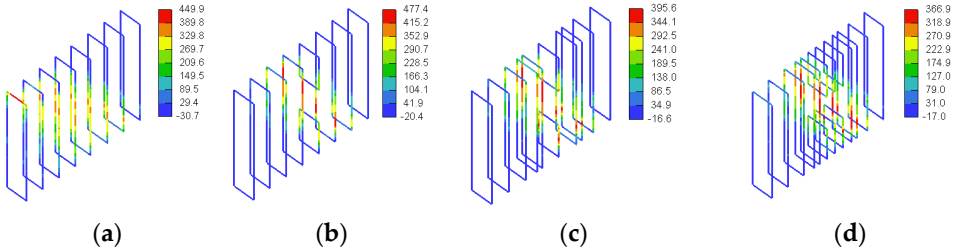

Figure 9. Three-dimensional view of stresses in vertical GFRP stirrups (MPa): (**a**) DB-S; (**b**) DB-O1; (**c**) DB-O2; (**d**) DB-O3.

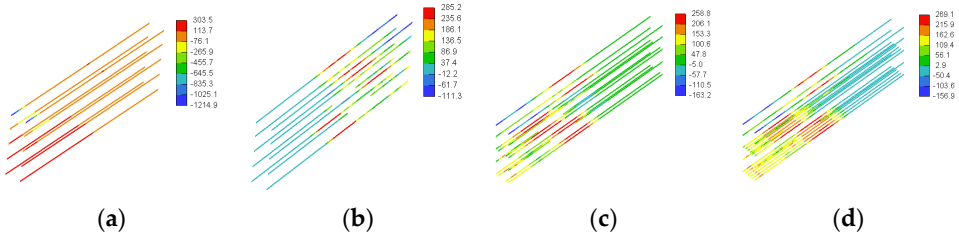

Figure 10. Three-dimensional view of stresses in horizontal web reinforcement (MPa): (**a**) DB-S; (**b**) DB-O1; (**c**) DB-O2; (**d**) DB-O3.

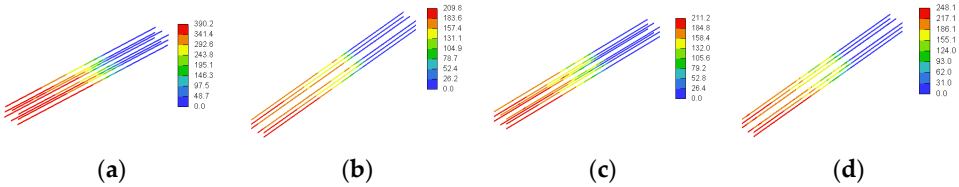

Figure 11. Three-dimensional view of stresses in flexural reinforcement (MPa): (**a**) DB-S; (**b**) DB-O1; (**c**) DB-O2; (**d**) DB-O3.

4. Parametric Study

Following the validation of the developed numerical models, a parametric study was conducted to study the effect of different opening sizes and locations on the shear behavior of GFRP-reinforced deep beams with a web opening. The parametric study was divided into two phases. The first phase focused on the analysis of deep beams with a web opening in the middle of the shear span having different sizes. The second phase focused on the analysis of deep beams with a web opening at different locations with respect to the natural load path within the shear span, noting that the natural load path is the line connecting the edges of the support plate and the load plate. The results of the parametric study include the load-deflection response, crack propagation, failure mechanism, and stresses in the GFRP reinforcement.

4.1. Deep Beam Models with Different Opening Sizes

Parameters of the deep beam models with different opening sizes are summarized in Table 3. The variables included values of w_o/a (0.16, 0.27, and 0.32) and values of h_o/h (0.17, 0.25, and 0.33). The deep beam models are labeled DB-WX-HY, where X denotes the value of w_o/a and Y refers to h_o/h. For instance, DB-W0.16-H0.25 is the designation of the deep beam model having a w_o/a of 0.16 and h_o/h of 0.25. Figures 12–14 show details of the reinforcement of the numerical models with different opening sizes in the middle of the shear span.

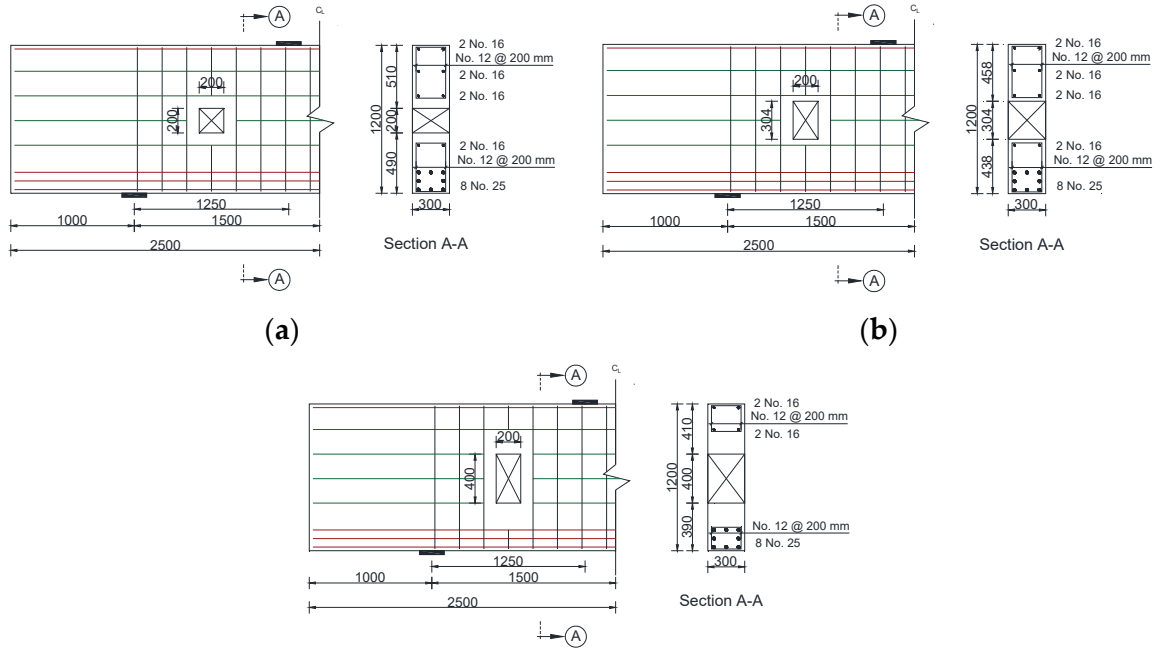

Figure 12. Details of deep beam models with w_o/a = 0.16, noting that bars with red, green, and black colors represent the main flexural reinforcement, the horizontal web reinforcement, and the vertical web reinforcement, respectively (dimensions are in mm): (**a**) h_o/h = 0.17; (**b**) h_o/h = 0.25; (**c**) h_o/h = 0.33.

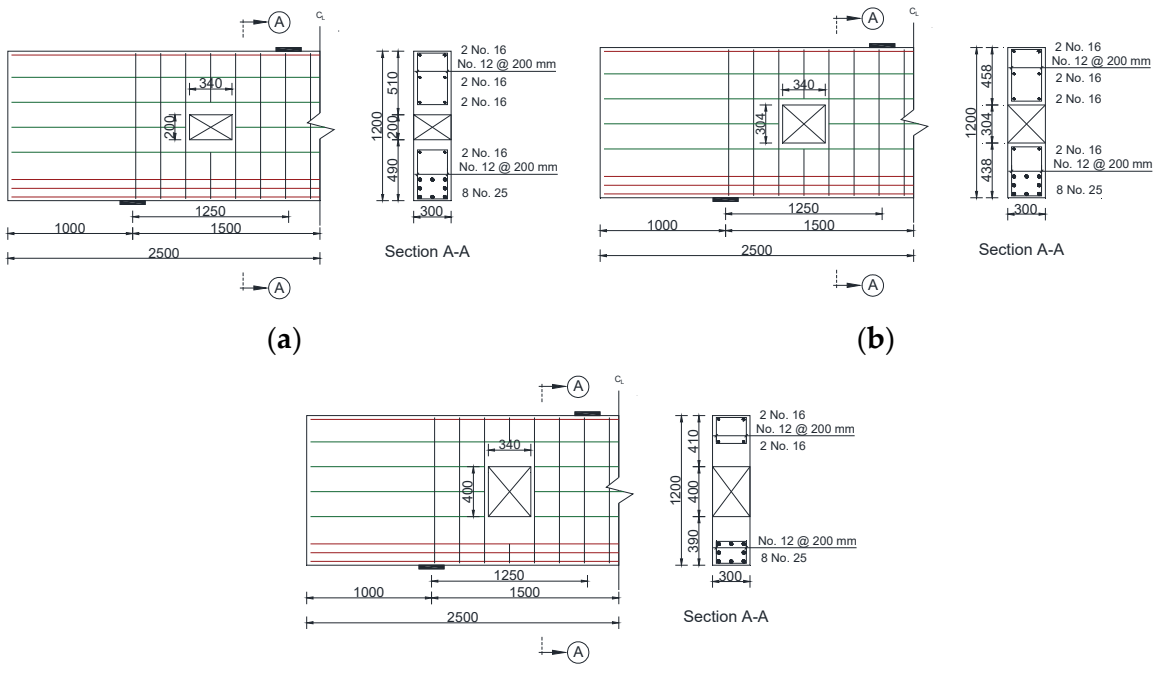

Figure 13. Details of deep beam models with w_o/a = 0.27, noting that bars with red, green, and black colors represent the main flexural reinforcement, the horizontal web reinforcement, and the vertical web reinforcement, respectively (dimensions are in mm): (**a**) h_o/h = 0.17; (**b**) h_o/h = 0.25; (**c**) h_o/h = 0.33.

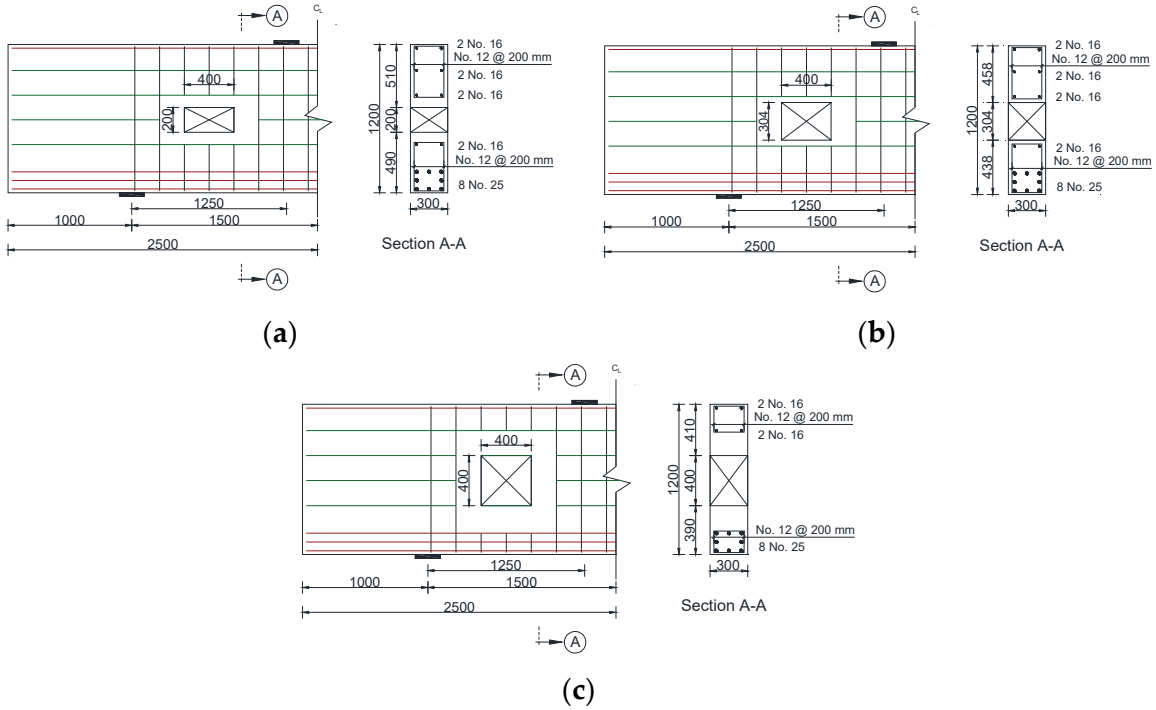

Figure 14. Details of deep beam models with w_o/a = 0.32, noting that bars with red, green, and black colors represent the main flexural reinforcement, the horizontal web reinforcement, and the vertical web reinforcement, respectively (dimensions are in mm): (**a**) h_o/h = 0.17; (**b**) h_o/h = 0.25; (**c**) h_o/h = 0.33.

Table 3. Parameters of deep beam models with different opening sizes.

Model Designation	Opening Size (mm)	
	w_o *	h_o **
DB-W0.16-H0.17	200	200
DB-W0.16-H0.25		304
DB-W0.16-H0.33		400
DB-W0.27-H0.17	340	200
DB-W0.27-H0.25		304
DB-W0.27-H0.33		400
DB-W0.32-H0.17	400	200
DB-W0.32-H0.25		304
DB-W0.32-H0.33		400

* w_o values of 200, 340, and 400 mm correspond to w_o/a values of 0.16, 0.27, and 0.32, respectively. ** h_o values of 200, 304, and 400 mm correspond to h_o/h values of 0.17, 0.25, and 0.33, respectively.

4.1.1. Load-Deflection Response

Figure 15a–c show the load-deflection responses of the deep beam models with a web opening of different sizes placed in the middle of the shear span. The response of the solid deep beam model was included in the figures for the purpose of comparison. The installation of the web opening in the middle of the shear span reduced the shear cracking load and the post-cracking stiffness relative to those of the solid deep beam model. An increase in the opening size further compromised the response of the beam models. The reductions in the cracking load and post-cracking stiffness caused by increasing the opening height were more pronounced for the models with the greater w_o/a of 0.32. The beam models with the web opening failed at a deflection significantly lower than that of the solid beam model DB-S.

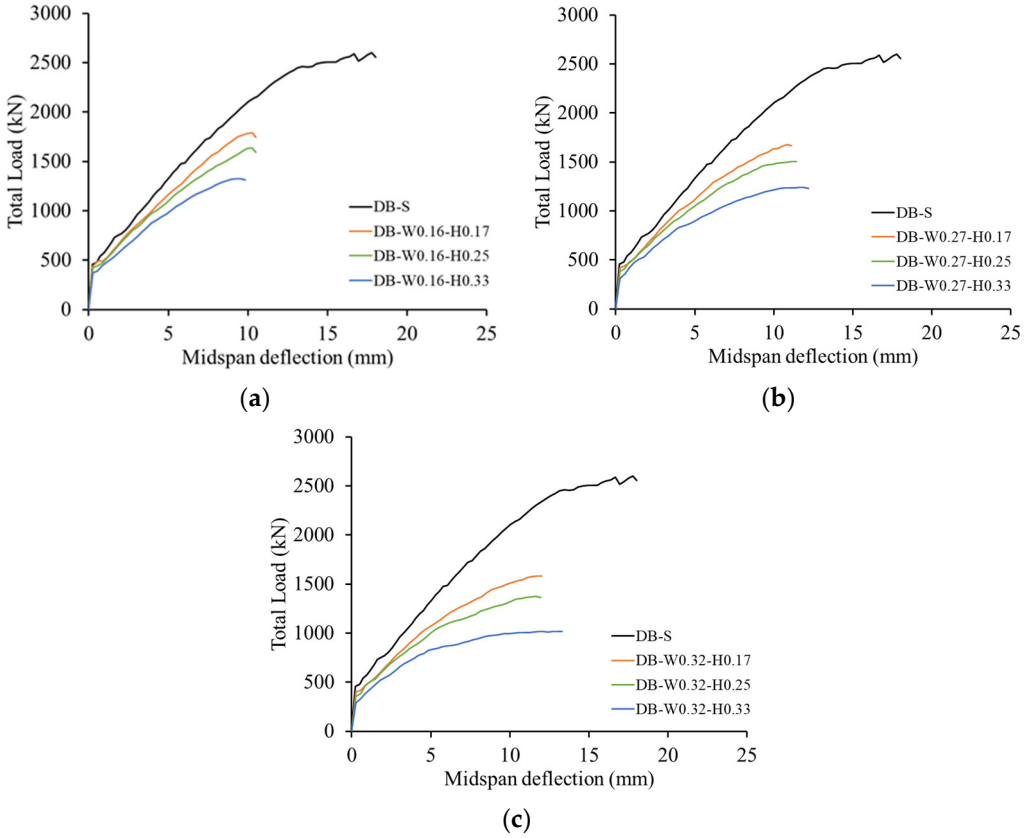

Figure 15. Effect of opening size on the load-deflection response: (**a**) w_o/a = 0.16; (**b**) w_o/a = 0.27; (**c**) w_o/a = 0.32.

Table 4 presents the ultimate load and the deflection at ultimate load for the beam models. At the same w_o/a of 0.16, strength reductions of 31, 37, and 49% were recorded for the deep beam models with h_o/h values of 0.17, 0.25, and 0.33, respectively. The strength reduction caused by increasing the opening height was more pronounced at the greater w_o/a values. At a w_o/a of 0.27, strength reductions of 35, 42, and 52% were recorded for the deep beam models with h_o/h values of 0.17, 0.25, and 0.33, respectively. At a w_o/a of 0.32, strength reductions of 39, 47, and 61% were recorded for the deep beam models with h_o/h values of 0.17, 0.25, and 0.33, respectively. Although the deflection capacity of the beam models with a web opening was significantly lower than that of the solid deep beam model, changing the opening size had a minor impact on the deflection capacity. The deflection capacities of the beam models with different opening heights were insignificantly different.

Table 4. Numerical results of the deep beam models with different opening sizes.

Model Designation	Opening Size (mm)		Ultimate Load (kN)	Deflection at Ultimate (mm)
	w_o	h_o		
DB-S	-	-	2601	17.8
DB-W0.16-H0.17	200	200	1789	10.3
DB-W0.16-H0.25		304	1637	10.3
DB-W0.16-H0.33		400	1327	9.5
DB-W0.27-H0.17	340	200	1678	10.8
DB-W0.27-H0.25		304	1504	11.2
DB-W0.27-H0.33		400	1239	11.9
DB-W0.32-H0.17	400	200	1585	11.7
DB-W0.32-H0.25		304	1374	11.7
DB-W0.32-H0.33		400	1019	13.0

The deflection capacities of the beam models with w_o/a values of 0.16, 0.27, and 0.32 were 56, 64, and 68% of those of the solid beam model DB-S. The strength of the beam models with web openings was normalized to that of the solid beam model DB-S, and then plotted against the opening size in Figure 16. It is evident that the strength of the beam models decreased with an increase in either the opening width or height. The rate of the strength reduction tended to be significant when the value of w_o/a increased from 0.27 and 0.32 (Figure 16a). Similarly, the strength degraded at a higher rate when the value of h_o/h increased from 0.25 and 0.33 as shown in Figure 16b. The rate of the strength reduction caused by increasing the opening height (Figure 16b) was, however, more significant than that produced by increasing the opening width (Figure 16a). It is noteworthy that the strength of deep beams with a web opening in the middle of the shear span typically decreases when reducing the angle of inclination of the lower load path connecting the edge of the support plate and the bottom corner of the opening nearest to the load plate (angle of inclination of crack D in Figure 8b) [36,37]. The increase in the opening height caused a greater reduction in the angle of inclination of the lower load path than that caused by increasing the opening width, which justifies the higher rate of strength reduction exhibited by the beam models with an increased opening height.

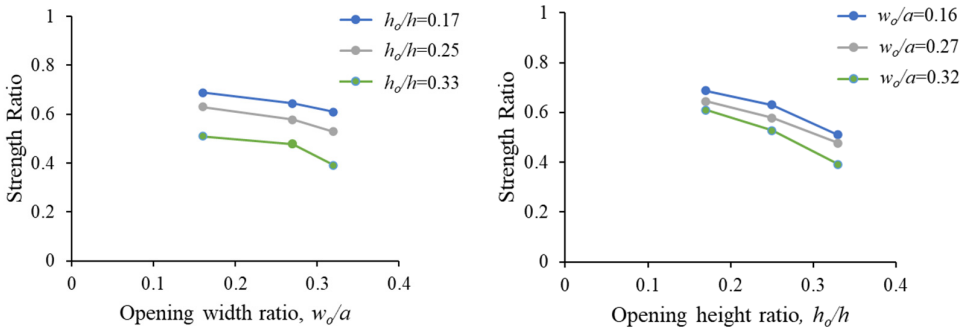

(**a**) (**b**)

Figure 16. Effect of the opening size on the strength: (**a**) effect of the opening width; (**b**) effect of the opening height.

4.1.2. Crack Pattern and Failure Mechanism

Figures 17–19 show the crack development and propagation at different stages of loading along with the final pattern for sample deep beam models having a web opening in the middle of the shear span. The first crack in all beam models of this group initiated at the opening corners closer to the support and load points. As the load progressed, these cracks propagated diagonally toward the support and load plates. Flexural cracks were also initiated at the midspan and within the shear span during loading, noting that the beam models DB-W0.32-H0.25 and DB-W0.32-H0.33 with the large web opening exhibited no or very few flexural cracks at a load value less than 50% of their peak loads. A further increase in the load resulted in the development of additional shear cracks in the top and bottom chords causing a band of shear cracks below and above the opening. The final failure was dependent on the opening size. The deep beam models with the opening widths of 200 and 340 mm, having respective w_o/a values of 0.16 and 0.27, failed due to the fracturing of the concrete along the lower load path connecting the edge of the support plate and the opposite corner of the opening in the bottom chord along with excessive widening of the shear crack at the opening corner. In most of the deep beam models with w_o/a values of 0.16 and 0.27, extensive shear cracks also developed along the upper load path in the top chord connecting the edge of the load plate to the opposite corner of the opening, causing failure along the upper load path simultaneously with that which occurred along the lower load path. It is noteworthy that the lower load path is vulnerable to failure before the upper load path because of the transverse strains caused by the stresses in the flexural tensile reinforcement at the bottom of the beam model. In contrast, the deep beam models with

the opening width of 400 mm, having a respective w_o/a of 0.32, failed due to the excessive widening of shear cracks at the opening corners closer to the load and support plates along with excessive rotation that occurred in the top and bottom chords.

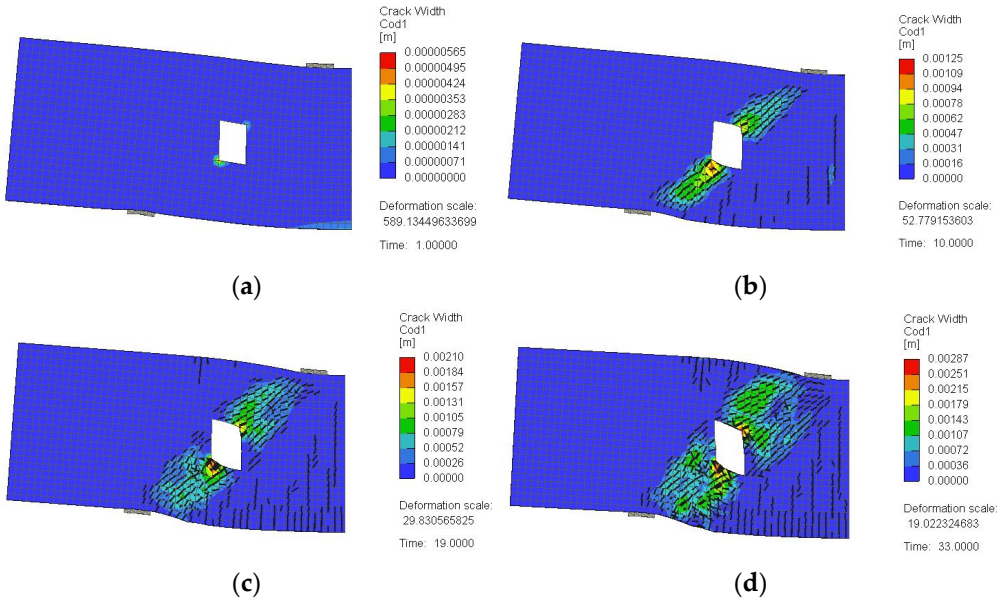

Figure 17. Crack pattern for a typical model failed along the lower load path (DB-W0.16-H0.25): (**a**) at 25% of peak load; (**b**) at 50% of peak load; (**c**) at 75% of peak load; (**d**) at 100% of peak load.

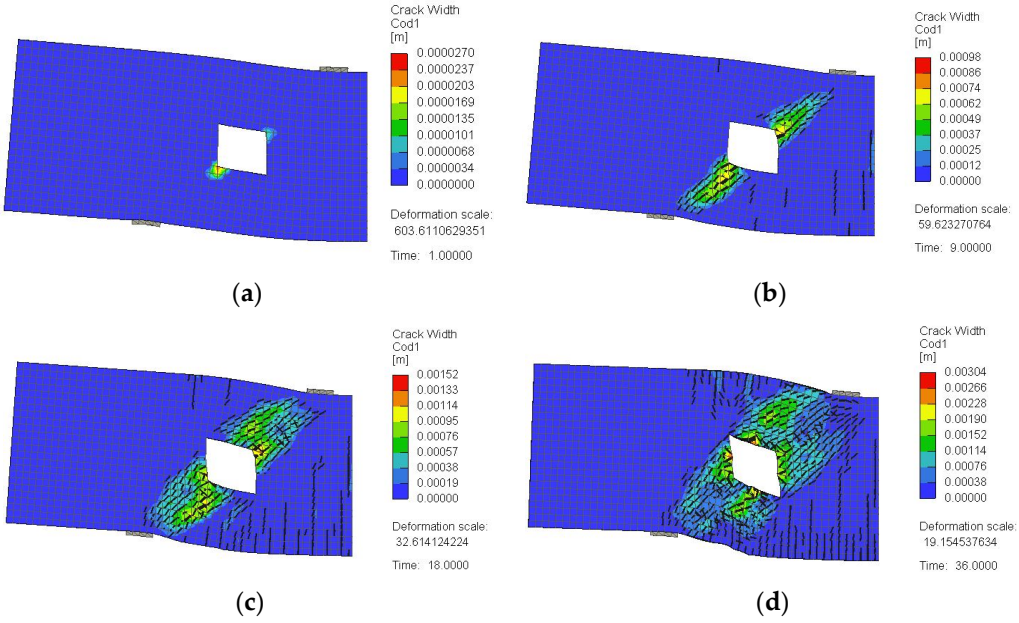

Figure 18. Crack pattern for a typical model failed along the lower and upper load path (DB-W0.27-H0.25): (**a**) at 25% of peak load; (**b**) at 50% of peak load; (**c**) at 75% of peak load; (**d**) at 100% of peak load.

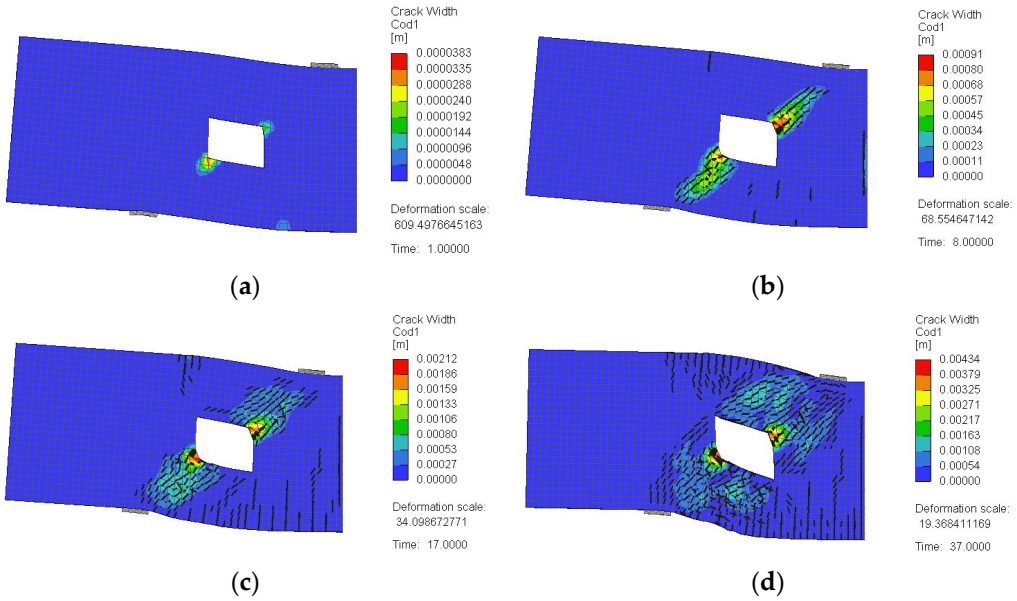

Figure 19. Crack pattern for a typical model failed due to an excessive widening of shear cracks at the opening corners (DB-W0.32-H0.25): (**a**) at 25% of peak load; (**b**) at 50% of peak load; (**c**) at 75% of peak load; (**d**) at 100% of peak load.

4.1.3. GFRP Stresses

General 3D views of the stresses in the vertical GFRP stirrups predicted numerically for the beam models of this group are shown in Figures 20–22. For the beam models with the smaller w_o/a value of 0.16, the maximum stresses in the vertical GFRP stirrups were in the straight portions of the stirrup near the corner of the web opening closer to the support plate (Figure 20). The maximum GFRP stress at peak load for DB-W0.16-H0.17 with w_o/a = 0.16 and h_o/h = 0.17 was 48% of the tensile strength of straight GFRP bars. The respective value for the other two models with the greater h_o/h values of 0.25 and 0.33 was, on average, 57% of the tensile strength of straight GFRP bars. For the beam models with w_o/a = 0.27, the maximum stresses in the vertical GFRP stirrups were in the straight portions of the stirrup near both corners of the web opening closer to the support and load plates (Figure 21). The maximum GFRP stresses at peak load for the beam models with w_o/a = 0.27 and h_o/h values of 0.17, 0.25, and 0.33 were 42, 47, and 54% of the tensile strength of straight GFRP bars, respectively. The vertical GFRP bars at the sides of the opening exhibited higher stresses in the beam models with the greater opening height because increasing the opening height reduced the contribution of the concrete to the shear resistance, and hence, higher stresses were transferred/resisted by the GFRP stirrups. For the beam models with the greatest w_o/a value of 0.32, the maximum stresses in the vertical GFRP stirrups were in the straight portions of the stirrup near the corner of the web opening closer to the support plate, except for DB-W0.32-H0.17, which exhibited maximum GFRP stresses at both corners of the web opening (Figure 22). The maximum GFRP stresses at peak load for the beam models with a w_o/a of 0.32 were in the range of 34 to 42% of the tensile strength of straight GFRP bars, and they also tended to increase with an increase in the opening height. In contrast, for the beam models with the same opening height and different opening widths, it can be seen that the stresses in the vertical GFRP stirrups at the sides of the opening decreases with an increase in the opening width. This behavior could be due to an increased transfer of shear stresses through the upper and lower chords for the beam models with the greater opening width. It is noteworthy that the stresses in the bottom portion of the vertical legs of the GFRP stirrup placed at the side of the opening closer to the support plate in most of the beam models with w_o/a values of 0.16 and 0.27 were in the range of 90 to 100% of the tensile strength of the bent portion of GFRP bars for the beam models. These results implied the possible rupture of these vertical GFRP

stirrups at the bent portions in most of the beam models with w_o/a values of 0.16 and 0.27. For the beam models with the greater w_o/a of 0.32, the stresses in the vertical GFRP bars were below the rupture strength of the bent portions of the GFRP bars.

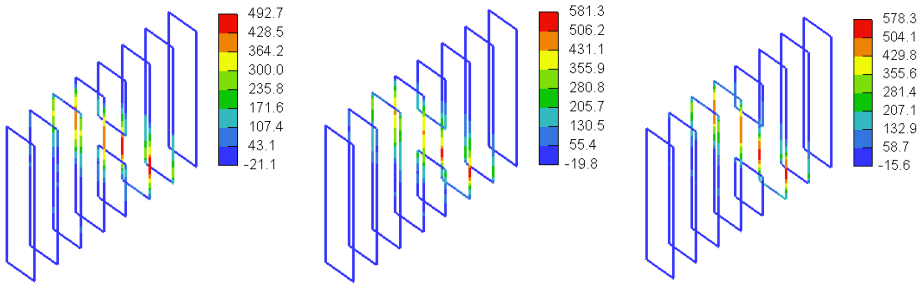

Figure 20. Three-dimensional view of stresses in GFRP bars for models with w_o/a = 0.16 (MPa): (**a**) DB-W0.16-H0.17; (**b**) DB-W0.16-H0.25; (**c**) DB-W0.16-H0.33.

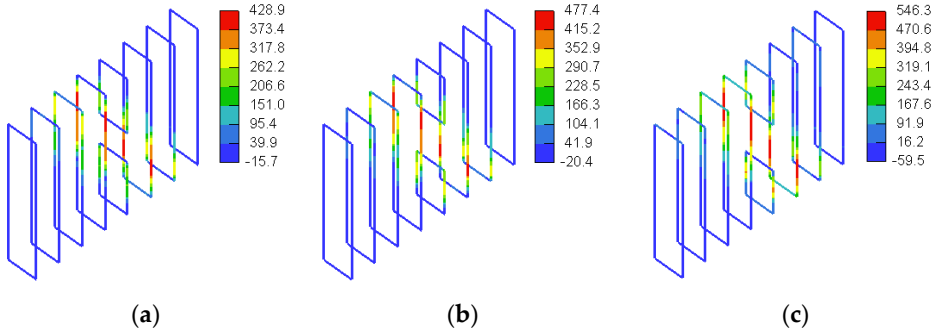

Figure 21. Three-dimensional view of stresses in GFRP bars for models with w_o/a = 0.27 (MPa): (**a**) DB-W0.27-H0.17; (**b**) DB-W0.27-H0.25; (**c**) DB-W0.27-H0.33.

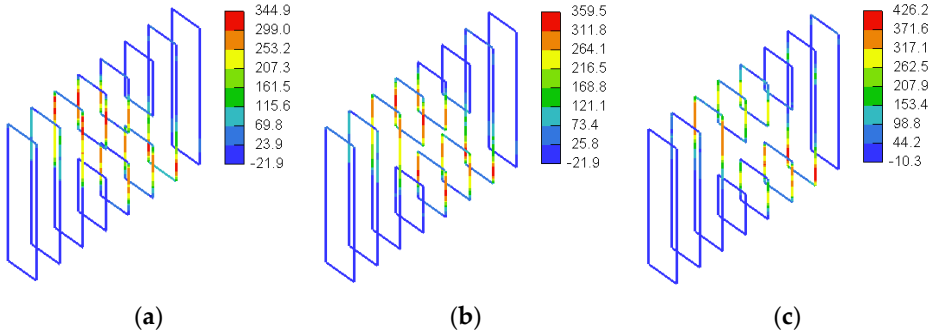

Figure 22. Three-dimensional view of stresses in GFRP bars for models with w_o/a = 0.32 (MPa): (**a**) DB-W0.32-H0.17; (**b**) DB-W0.32-H0.25; (**c**) DB-W0.32-H0.33.

None of the horizontal web reinforcing bars or the flexural reinforcement at the tension side in the deep beam models of this group reached their tensile strength. The stresses in the horizontal web reinforcement and tensile flexural reinforcement predicted numerically for the beam models of this group are shown in Figures 23–28. For the beam models with the smaller w_o/a value of 0.16, the maximum stresses in the horizontal web reinforcement were on average 258 MPa, which corresponded to 22% of the tensile strength of the GFRP bars (Figure 23). The maximum stress in their tensile flexural reinforcement ranged from 190 to 249 MPa, which corresponds to 19 to 25% of the tensile strength of the GFRP bars (Figure 24). The beam models with the w_o/a value of 0.27 exhibited maximum stresses of 240 to 348 MPa (i.e., 21 to 30% of the tensile strength of the GFRP bars) in the horizontal web reinforcement and 200 to 236 MPa (i.e., 20 to 24% of the tensile strength of the GFRP

bars) in the tensile flexural reinforcement as shown in Figures 25 and 26, respectively. The beam models with the w_o/a value of 0.32 exhibited maximum stresses of 324 to 382 MPa (i.e., 27 to 38% of the tensile strength of the bars) in the horizontal web reinforcement and 169 to 226 MPa (i.e., 17 to 23% of the tensile strength of the GFRP bars) in the tensile GFRP flexural reinforcement as shown in Figures 27 and 28, respectively. These results indicate that for the beam models with the web opening in the middle of the shear span, varying the opening size had an insignificant effect on the maximum stresses of the horizontal web reinforcement and tensile flexural reinforcement recorded at peak load. Generally, the maximum stresses recorded in the horizontal web reinforcement were in the range of 21 to 38% of the GFRP tensile strength, whereas those of the tensile flexural reinforcement were in the range of 19 to 25% of the GFRP tensile strength.

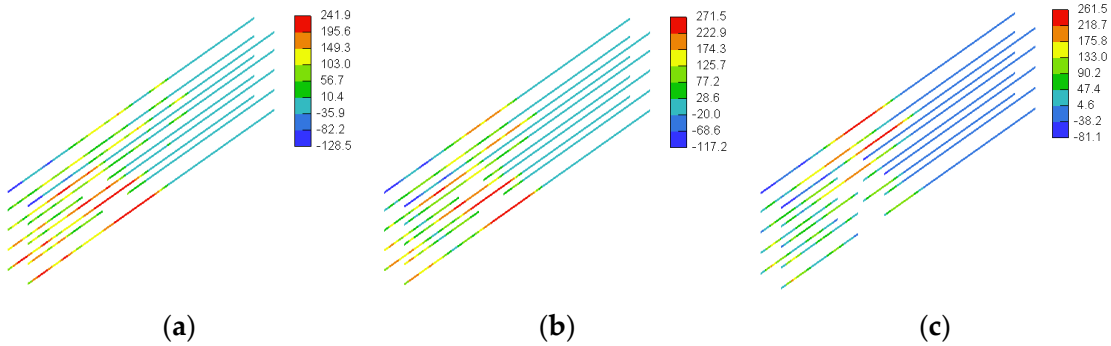

Figure 23. Stresses in horizontal GFRP web reinforcement for models with w_o/a = 0.16 (MPa): (**a**) DB-W0.16-H0.17; (**b**) DB-W0.16-H0.25; (**c**) DB-W0.16-H0.33.

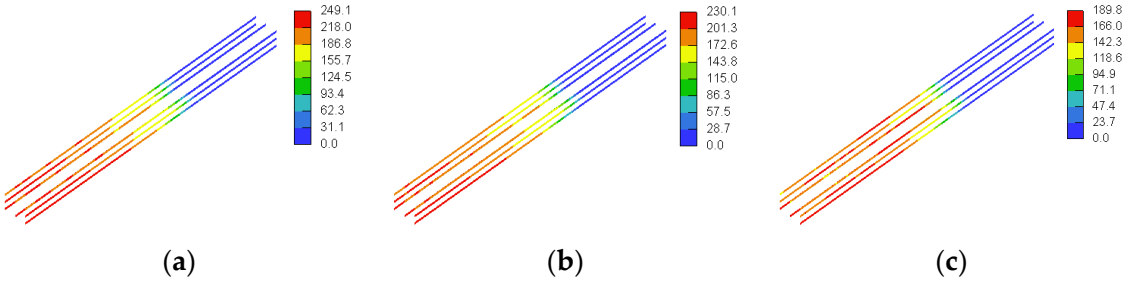

Figure 24. Stresses in bottom GFRP flexural reinforcement for models with w_o/a = 0.16 (MPa): (**a**) DB-W0.16-H0.17; (**b**) DB-W0.16-H0.25; (**c**) DB-W0.16-H0.33.

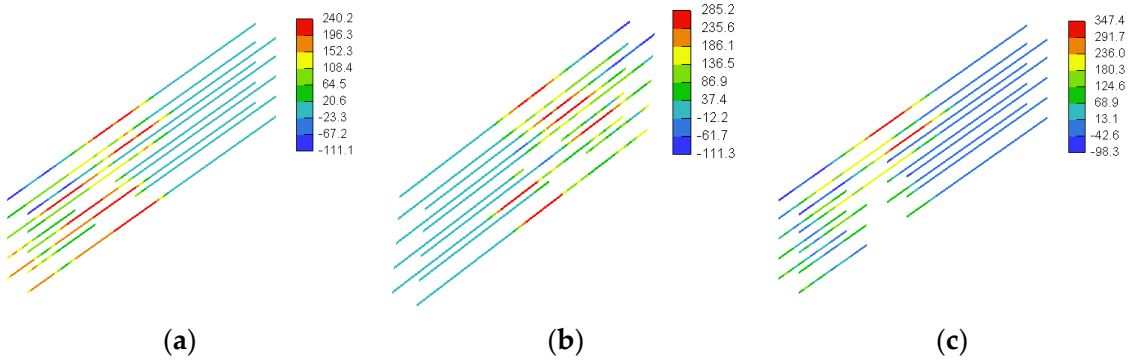

Figure 25. Stresses in horizontal GFRP web reinforcement for models with w_o/a = 0.27 (MPa): (**a**) DB-W0.27-H0.17; (**b**) DB-W0.27-H0.25; (**c**) DB-W0.27-H0.33.

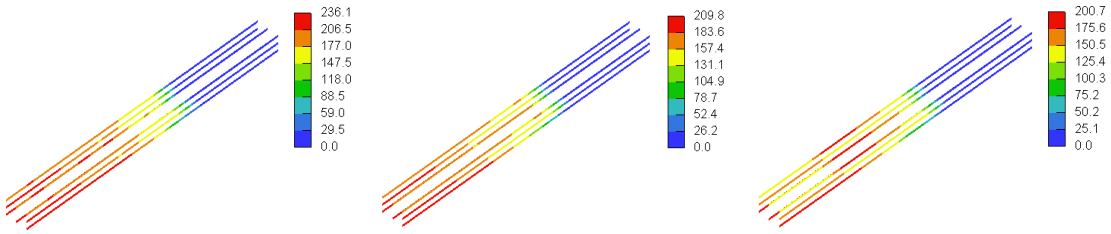

Figure 26. Stresses in bottom GFRP flexural reinforcement for models with w_o/a = 0.27 (MPa): (**a**) DB-W0.27-H0.17; (**b**) DB-W0.27-H0.25; (**c**) DB-W0.27-H0.33.

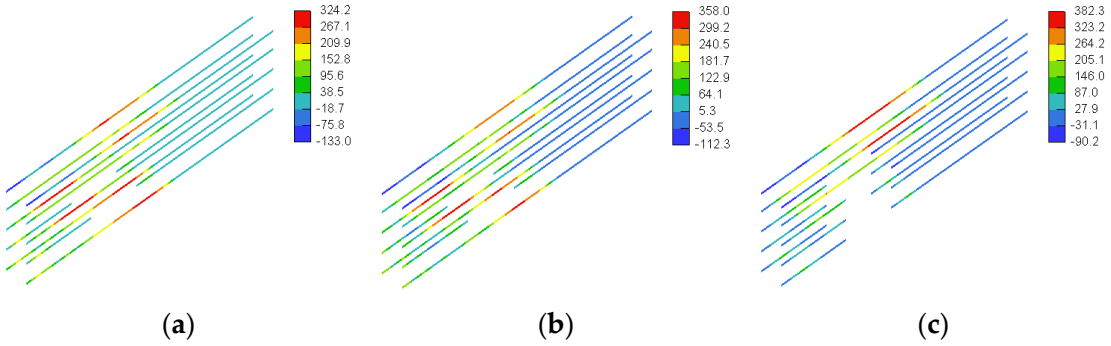

Figure 27. Stresses in horizontal GFRP web reinforcement for models with w_o/a = 0.32 (MPa): (**a**) DB-W0.27-H0.17; (**b**) DB-W0.27-H0.25; (**c**) DB-W0.27-H0.33.

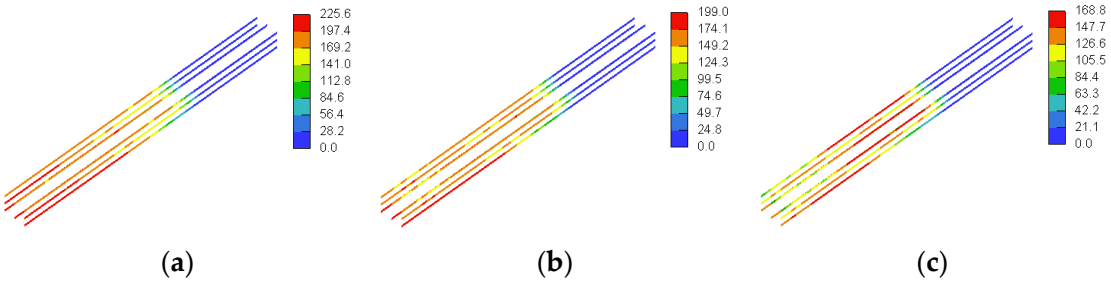

Figure 28. Stresses in bottom GFRP flexural reinforcement for models with w_o/a = 0.32 (MPa): (**a**) DB-W0.32-H0.17; (**b**) DB-W0.32-H0.25; (**c**) DB-W0.32-H0.33.

4.2. Deep Beam Models with Different Opening Locations

The parameters of the deep beam models with different opening locations are summarized in Table 5. The deep beam models of this group had the same web opening size of w_o = 340 mm and h_o = 304 mm (i.e., w_o/a = 0.27 and h_o/h = 0.25). The primary variable of this group was the location of the web opening. The center of the web opening was located at a distance x_o from the face of the support plate and y_o from the bottom soffit of the beam model. The locations of the center of the opening in the horizontal and vertical directions were normalized to the clear shear span (X_c) and beam depth (h), respectively. Values of the term x_o/X_c were 0.25, 0.50, and 0.75, whereas those of the term y_o/h were 0.33, 0.50, and 0.75. The deep beam models are labeled DB-WM-HN, where M denotes the value of x_o/X_c and N refers to y_o/h. For instance, DB-X0.25-Y0.33 is the designation of the deep beam model having x_o/X_c of 0.25 and y_o/h 0.33. Figures 29–31 show details of the reinforcement for the beam models of this group.

Table 5. Parameters of deep beam models with different opening locations.

Model Designation	Opening Location (mm)	
	x_o *	y_o **
DB-X0.25-Y0.33	262.5	400
DB-X0.25-Y0.50		590
DB-X0.25-Y0.75		900
DB-X0.50-Y0.33	525	400
DB-X0.50-Y0.50		590
DB-X0.50-Y0.75		900
DB-X0.75-Y0.33	787.5	400
DB-X0.75-Y0.50		590
DB-X0.75-Y0.75		900

* x_o values of 262.5, 525, and 787.5 mm correspond to x_o/X_c values of 0.25, 0.50, and 0.75, respectively. ** y_o values of 400, 590, and 900 mm correspond to y_o/h values of 0.33, 0.50, and 0.75, respectively.

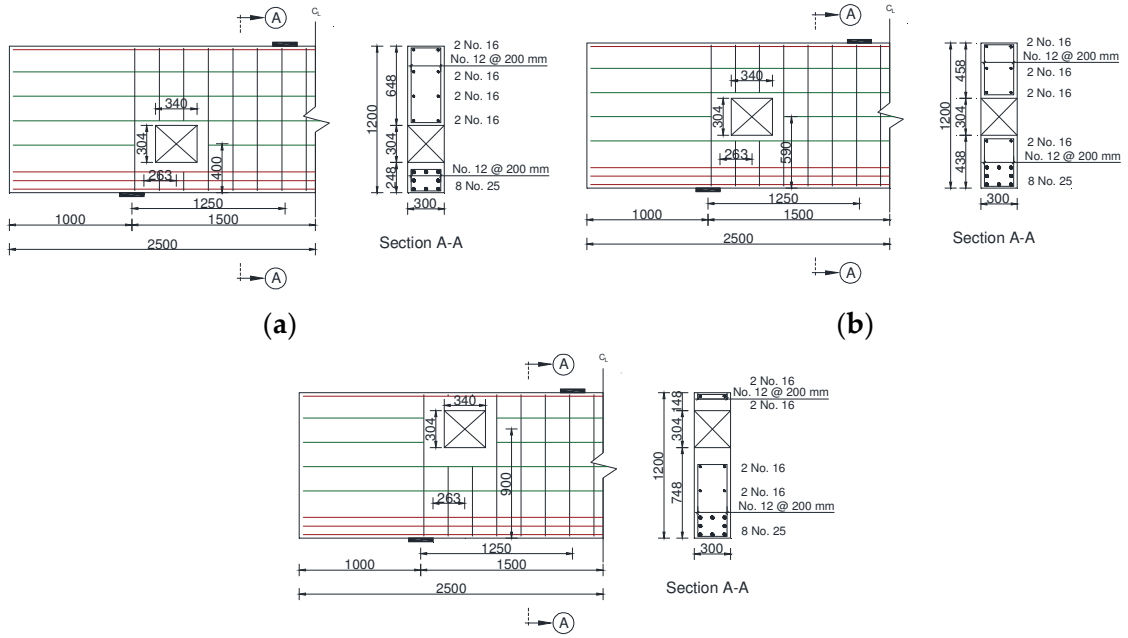

Figure 29. Details of deep beam models with x_o/X_c = 0.25, noting that bars with red, green, and black colors represent the main flexural reinforcement, the horizontal web reinforcement, and the vertical web reinforcement, respectively (dimensions are in mm): (**a**) y_o/h = 0.33; (**b**) y_o/h = 0.50; (**c**) y_o/h = 0.75.

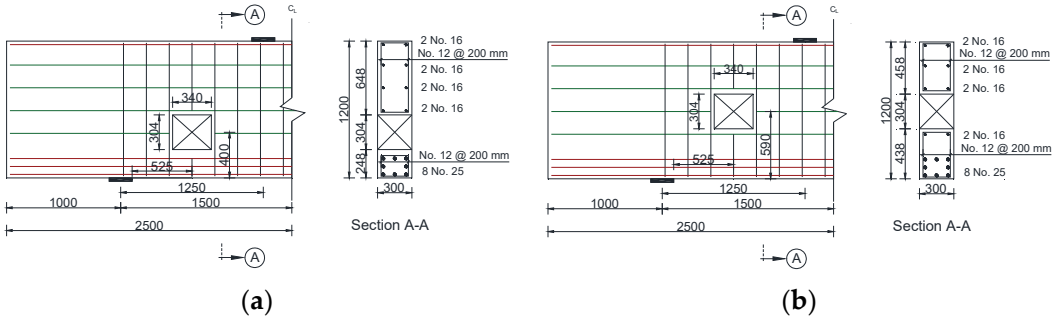

Figure 30. *Cont.*

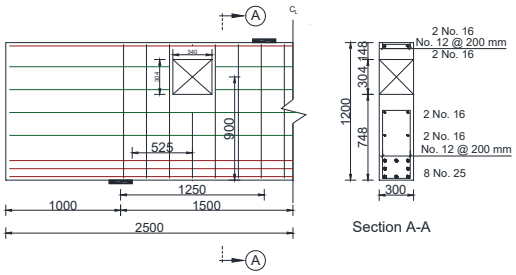

(**c**)

Figure 30. Details of deep beam models with x_o/X_c = 0.50, noting that bars with red, green, and black colors represent the main flexural reinforcement, the horizontal web reinforcement, and the vertical web reinforcement, respectively (dimensions are in mm): (**a**) y_o/h = 0.33; (**b**) y_o/h = 0.50; (**c**) y_o/h = 0.75.

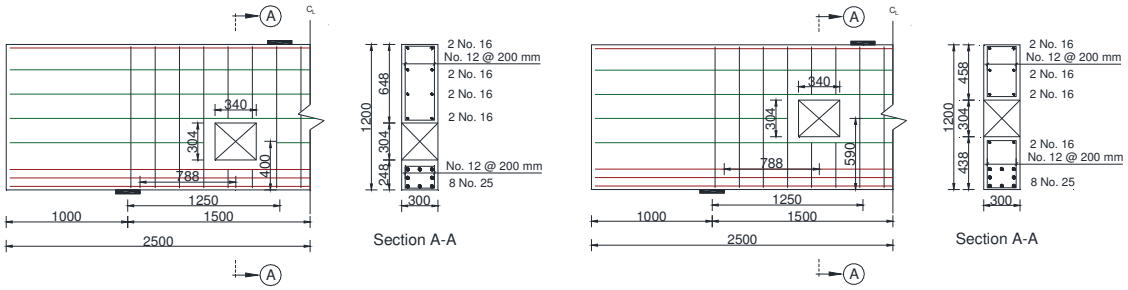

(**a**) (**b**)

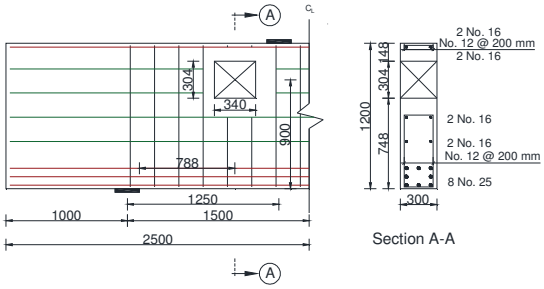

(**c**)

Figure 31. Details of deep beam models with x_o/X_c = 0.75 and different opening vertical locations, noting that bars with red, green, and black colors represent the main flexural reinforcement, the horizontal web reinforcement, and the vertical web reinforcement, respectively (dimensions are in mm): (**a**) y_o/h = 0.33; (**b**) y_o/h = 0.50; (**c**) y_o/h = 0.75.

4.2.1. Load-Deflection Response

Figure 32a–c show the load-deflection responses of the deep beam models with a web opening having an x_o/X_c of 0.25, 0.50, and 0.75 respectively. The response of the solid deep beam model DB-S is included in the figures for the purpose of comparison. Figure 32a shows that installation of the web opening near the support at an x_o/X_c of 0.25 seriously impaired the response of the beam models. The detrimental effect of the web opening was more pronounced for the beam models DB-X0.25-Y0.33 and DB-X0.25-Y0.50 with the lower y_o/h values of 0.33 and 0.50, respectively, because the opening in these two models fully interrupted the natural load path. The web opening in the beam model DB-X0.25-Y0.75 did not interrupt the natural load path, and hence, its post-cracking stiffness was almost the same as that of DB-S. The beam model DB-X0.25-Y0.75 failed, however, at lower load and deflection capacities than those of DB-S. Although the web opening in DB-X0.25-Y0.75 did not interrupt the natural load path, it could have affected the width of the middle portion

of a bottle-shaped strut that could have formed in the shear span. In addition, placing the web opening in the compression zone above the natural load path hindered the transfer of the load to the support through other struts formed above the natural load path. Figure 32b shows that the behavior of the beam models with the web opening installed at an x_o/X_c of 0.50 was affected by the location of the center of the opening with respect to the bottom face of the beam (y_o). Although the behavior of all models was inferior to that of the solid deep beam model DB-S, the degradation in the behavior intensified with an increase in the distance between the center of the opening and the bottom face of the beam. These results indicate that placing the web opening above the natural load path was more detrimental to the structural behavior than placing it below the natural load path. The presence of a web opening in the compression zone above the natural load path interrupted the formation of struts in this region, and hence, compromised the structural response. Figure 32c shows that the behavior of the beam models with the web opening installed at x_o/X_c of 0.75 was seriously affected by the location of the center of the opening in the vertical direction (y_o). The behavior of the beam model DB-X0.75-Y0.33 was not seriously affected by the opening since it was provided at the tension side (y_o/h = 0.33) away from the natural load path. In contrast, the behavior of the beam model DB-X0.75-Y0.75 with y_o/h = 0.75 was seriously compromised since the opening was very close to the load plate and fully interrupted the natural load path. Initially, the behavior of the beam model DB-X0.75-Y0.50 with y_o/h = 0.50 almost coincided with that of DB-X0.75-Y0.33 with y_o/h = 0.33 until the load reached a value of approximately 1250 kN. Next, a degradation in the behavior of the beam model DB-X0.75-Y0.50 occurred until it failed at load and deflection capacities lower than those of DB-X0.75-Y0.33. It is noteworthy that a change in the slope of the load-deflection response was observed prior to reaching the ultimate load, probably because of the development of new major cracks.

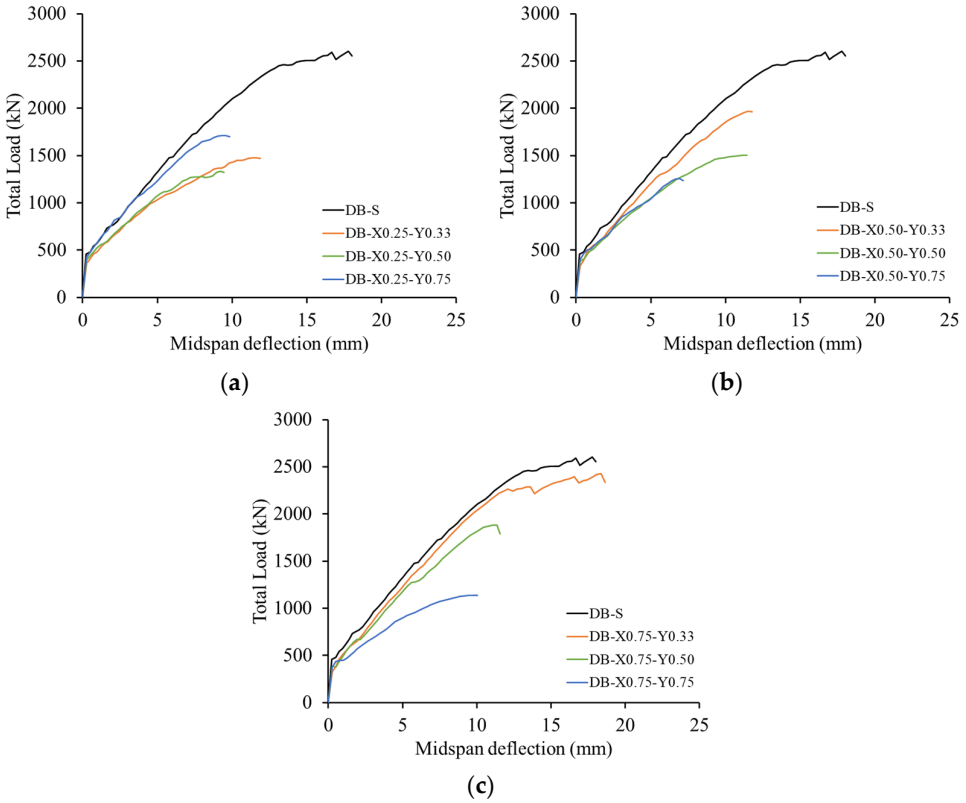

Figure 32. Effect of opening location on the load-deflection response: (**a**) x_o/X_c = 0.25; (**b**) x_o/X_c = 0.50; (**c**) x_o/X_c = 0.75.

Table 6 presents the ultimate load and the deflection capacity for the beam models of this group. For the beam models having a web opening with an x_o/X_c of 0.25, strength reductions of 43 and 49% were recorded for DB-X0.25-Y0.33 and DB-X0.25-Y0.50 having y_o/h values of 0.33 and 0.50, respectively. It is noteworthy that the web opening in DB-X0.25-Y0.33 and DB-X0.25-Y0.50 fully interrupted the natural load path. When the opening was pushed upward away from the natural load path in DB-X0.25-Y0.75, a lower strength reduction of 34% was recorded. The deflection capacity of the beam models containing a web opening with an x_o/X_c of 0.25 was, on average, 57% of that of DB-S. For the beam models having a web opening with an x_o/X_c of 0.50, strength reductions of 24, 42, and 52% were recorded for DB-X0.50-Y0.33, DB-X0.50-Y0.50, and DB-X0.50-Y0.75 having y_o/h values of 0.33, 0.50, and 0.75, respectively. These results indicate that the strength reduction for the beam models with an x_o/X_c = 0.5 was intensified with an increase in the distance between the center of the opening and the bottom face of the beam, noting that the opening in these three models interrupted the natural load path. The reduction in the ultimate load was accompanied by a reduction in the corresponding deflection capacity of 35 to 61%. For the beam models having a web opening with an x_o/X_c of 0.75, strength reductions of 7, 28, and 56% were recorded for DB-X0.75-Y0.33, DB-X0.75-Y0.50, and DB-X0.75-Y0.75 having y_o/h values of 0.33, 0.50, and 0.75, respectively. The beam model DB-X0.75-Y0.33 exhibited a negligible strength reduction of 7% because the web opening was in the tension side and did not interrupt the natural load path. In contrast, the beam model DB-X0.75-Y0.75 exhibited a significant strength reduction of 56% because the web opening was in the compression zone close to the load plate and fully interrupted the natural load path. The deflection capacity of DB-X0.75-Y0.33 with a y_o/h of 0.33 was almost the same as that of DB-S. Conversely, the beam model DB-X0.75-Y0.75 with a y_o/h of 0.75 exhibited a 45% reduction in the deflection capacity relative to that of DB-S.

Table 6. Numerical results of the deep beam models with different opening locations.

Model Designation	Opening Location (mm)		Ultimate Load (kN)	Deflection at Ultimate (mm)
	x_o *	y_o **		
DB-S	-	-	2601	17.8
DB-X0.25-Y0.33	262.5	400	1478	11.6
DB-X0.25-Y0.50		590	1337	9.2
DB-X0.25-Y0.75		900	1714	9.6
DB-X0.50-Y0.33	525	400	1971	11.5
DB-X0.50-Y0.50		590	1504	11.2
DB-X0.50-Y0.75		900	1259	6.9
DB-X0.75-Y0.33	787.5	400	2429	18.4
DB-X0.75-Y0.50		590	1881	11.4
DB-X0.75-Y0.75		900	1139	9.7

* x_o values of 262.5, 525, and 787.5 mm correspond to x_o/X_c values of 0.25, 0.50, and 0.75, respectively. ** y_o values of 400, 590, and 900 mm correspond to y_o/h values of 0.33, 0.50, and 0.75, respectively.

The relationships between the strength reduction caused by the web opening and the opening location are provided in Figure 33. For the beam models with a y_o/h of 0.33 and 0.50, the strength increased with an increase in the horizontal distance measured from the face of the support within the shear span. The strength of the beam models with a y_o/h of 0.33 tended to be higher than that of their counterparts with a y_o/h of 0.50, and this behavior was more evident with an increase in the distance from the face of the support plate. The opening in the beam models with a y_o/h = 0.33 was just above the longitudinal reinforcement in the tension side, which is already cracked due to the tensile stresses in the flexural reinforcement that act as a tie. Moving the opening in the beam models with

y_o/h = 0.33 in the horizontal direction away from the support plate reduced its interruption for the natural load path, and hence, increased the beam strength. The beam models with a y_o/h of 0.75 exhibited an opposite trend, where the strength decreased with an increase in the distance measured from the face of the support within the shear span. Moving the opening in the beam models with y_o/h = 0.75 in the horizontal direction away from the support plate increased its interruption for the natural load path, and hence, reduced the beam strength. These results verified the detrimental effect of placing a web opening in the compression zone closer to the load plate (x_o/X_c = 0.75 and y_o/h = 0.75). The results also implied that a negligible strength reduction could be obtained when the web opening was placed in the tension side above the flexural reinforcement but away from the natural load path and the support plate (x_o/X_c = 0.75 and y_o/h = 0.33).

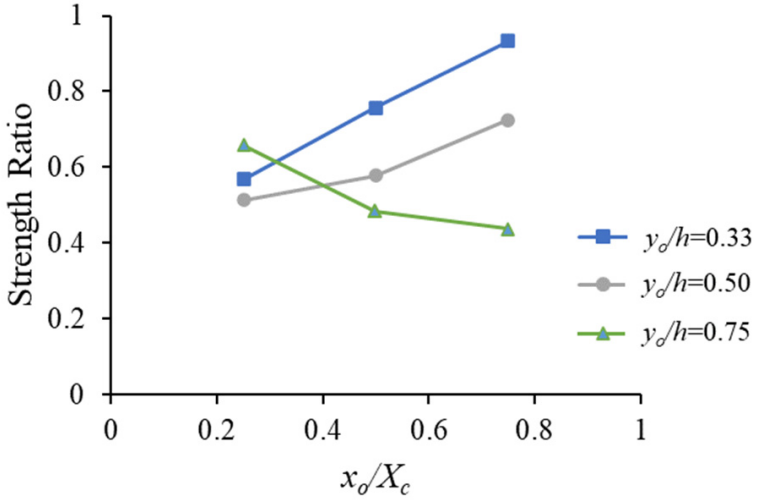

Figure 33. Effect of the opening location on the strength.

4.2.2. Crack Pattern and Failure Mechanism

Figures 34–37 show the crack development and propagation at different stages of loading along with the final pattern for sample deep beam models of this group. The beam models of this group, except those with the web opening close to the compression face of the beam (y_o/h = 0.75), exhibited first cracking at the opposite corner of the opening closer to the support and load points at a load value $\leq$ 25% of their strength. The beam models with y_o/h = 0.75 exhibited very few flexural cracks at 25% of the strength, whereas shear cracks were initiated at the opening corners at a load value higher than 25% of the strength. The shear cracks initiated earlier at the opening corners propagated diagonally toward the support and load plates as the load progressed. Flexural cracks were also initiated at the midspan, within the shear span, and in the bottom chord below the opening. Additional shear cracks were developed with an increase in the applied load creating a band of shear cracks. The final crack pattern and failure mode was dependent on the location of the opening. The beam models with the web opening away from the natural load path (DB-X0.25-Y0.75 and DB-X0.75-Y0.33) exhibited failure of the diagonal strut connecting the load and support plates. The beam model DB-X0.75-Y0.50 failed due to extensive diagonal shear cracking crossing the opening center. Other beam models failed due to the development of extensive diagonal cracks that caused the failure of the concrete along the upper and lower load paths or failure of the concrete along one of them combined with extensive diagonal cracks along the other load path as well as excessive widening of shear cracks at the opening corners.

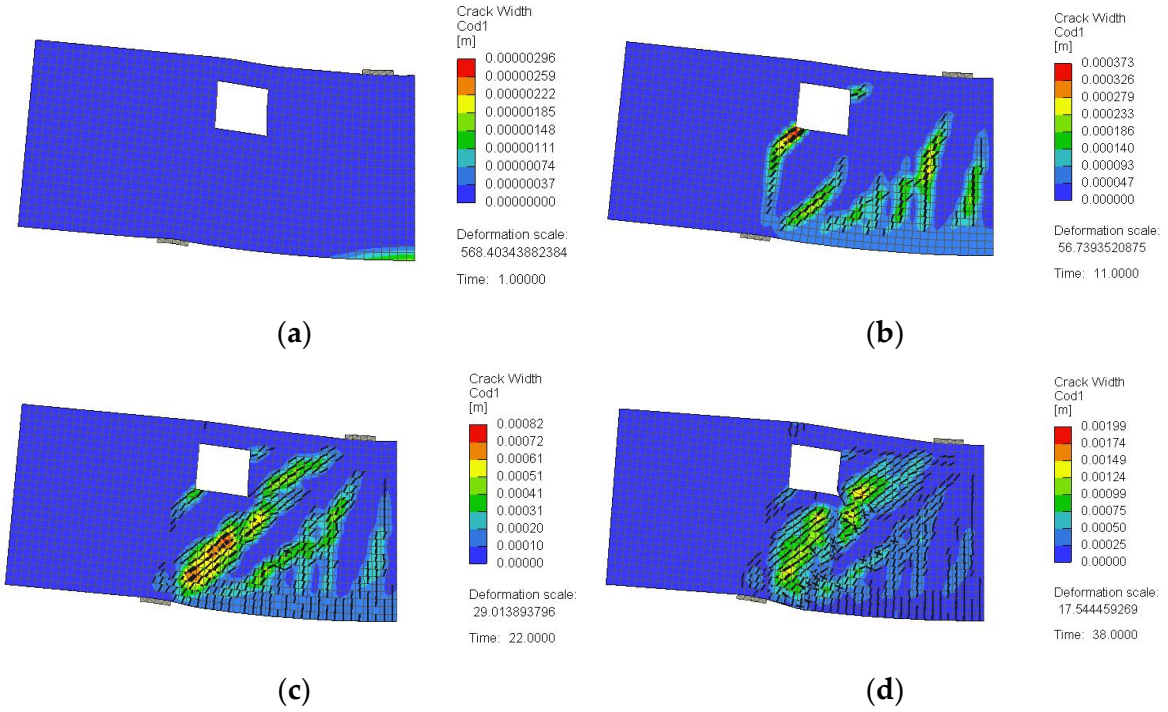

Figure 34. Crack pattern for a typical model that failed along the strut connecting the load and support plates (DB-X0.25-Y0.75): (**a**) at 25% of peak load; (**b**) at 50% of peak load; (**c**) at 75% of peak load; (**d**) at 100% of peak load.

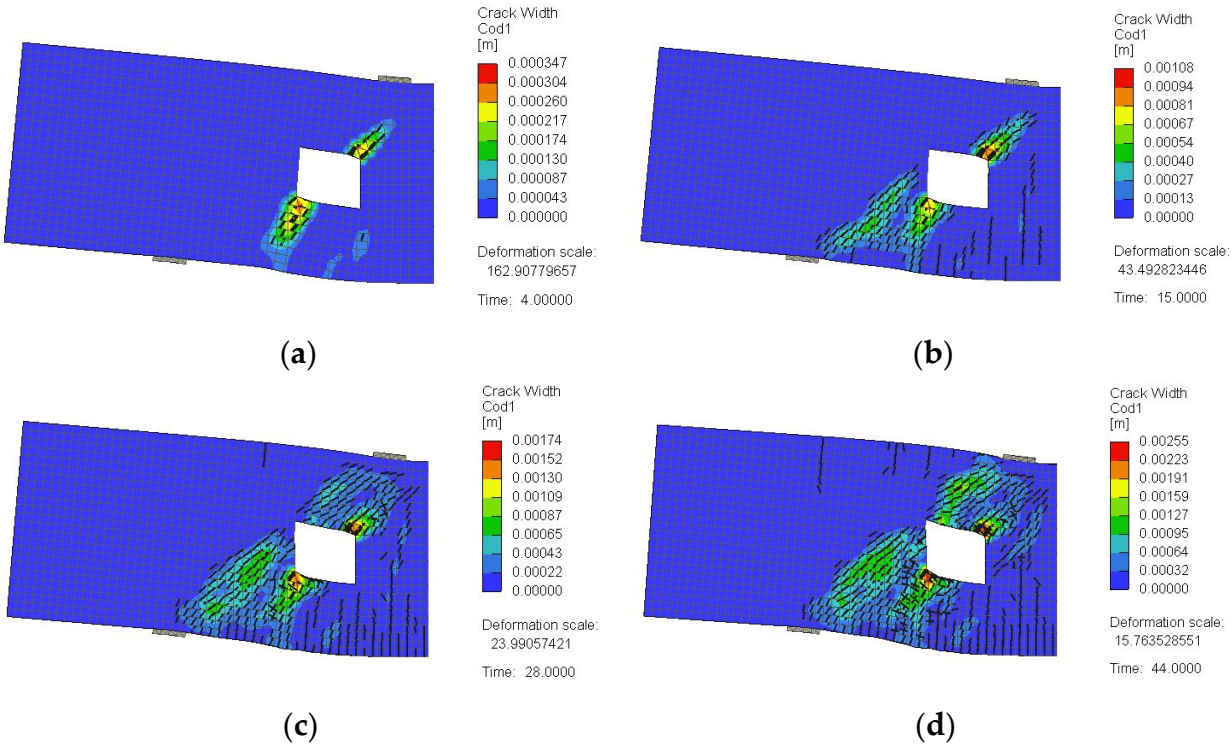

Figure 35. Crack pattern for a typical model that failed due to extensive diagonal shear cracking at the opening corners (DB-X0.75-Y0.50): (**a**) at 25% of peak load; (**b**) at 50% of peak load; (**c**) at 75% of peak load; (**d**) at 100% of peak load.

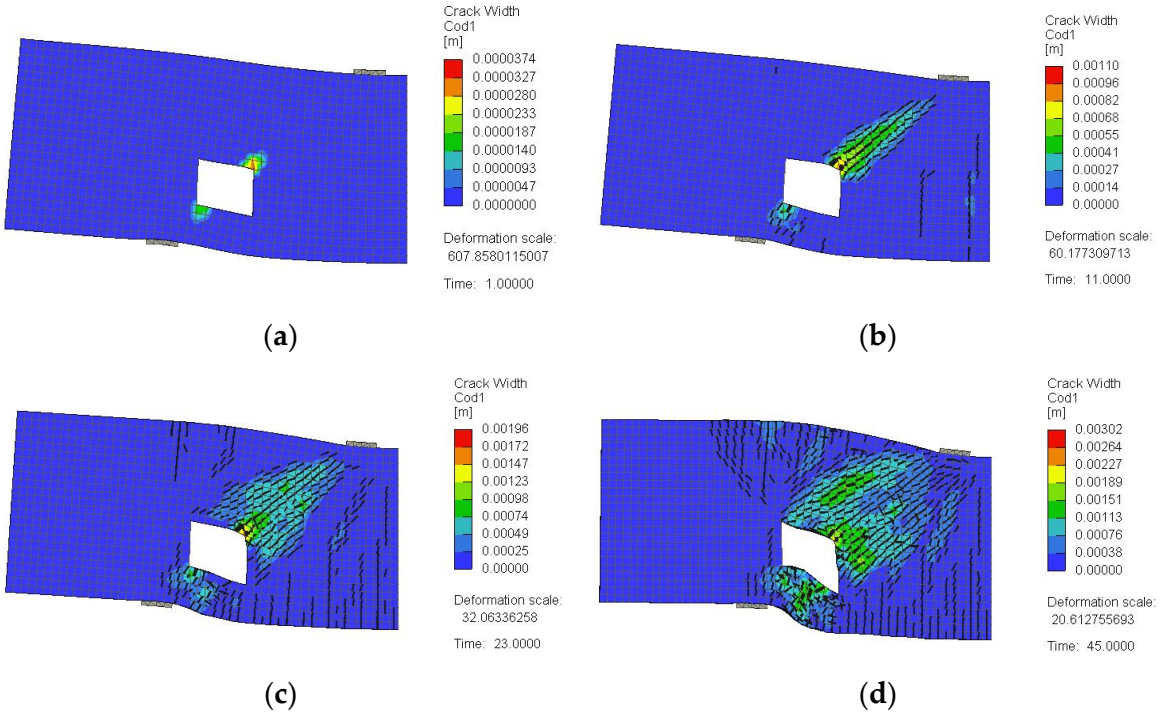

Figure 36. Crack pattern for a typical model that failed due to simultaneous failure of the concrete along the upper and lower load paths (DB-X0.25-Y0.33): (**a**) at 25% of peak load; (**b**) at 50% of peak load; (**c**) at 75% of peak load; (**d**) at 100% of peak load.

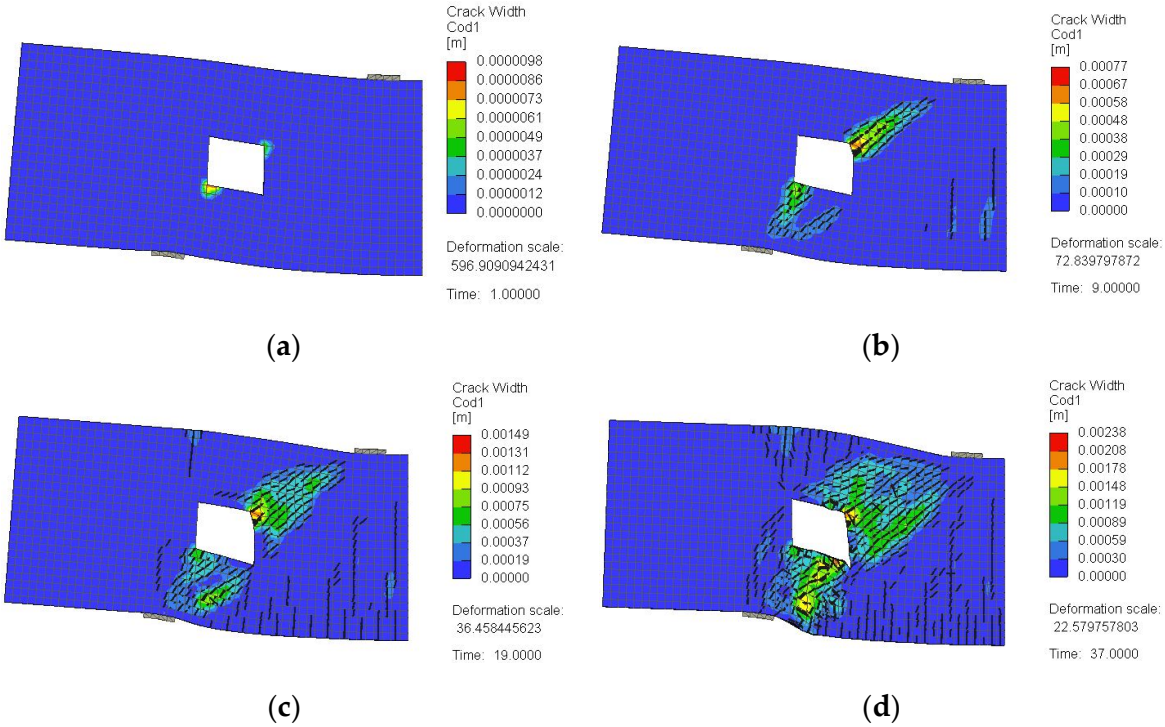

Figure 37. Crack pattern for a typical model that failed due to failure of the concrete along the lower load path and excessive widening of shear cracks at the opening corner (DB-X0.25-Y0.50): (**a**) at 25% of peak load; (**b**) at 50% of peak load; (**c**) at 75% of peak load; (**d**) at 100% of peak load.

4.2.3. GFRP Stresses

General 3D views of the stresses in the vertical GFRP stirrups predicted numerically for the beam models of this group are shown in Figures 38–40. The maximum stress in the vertical GFRP stirrups did not exceed the tensile strength of the bent portion (459 MPa), except in model DB-X0.50-Y0.50, which exhibited a maximum stress of 477 MPa in a location close to the bent portion. For the beam models with x_o/X_c = 0.25 (Figure 38), the maximum stress in the vertical GFRP stirrups ranged from 335 to 431 MPa. The location of the maximum stress in the vertical GFRP stirrups varied based on the value of y_o/h. When the opening was close to the tension face (DB-X0.25-Y0.33), the maximum stress was in the vertical GFRP stirrup at the side of the opening. When the opening was pushed upward (DB-X0.25-Y0.50 and DB-X0.25-Y0.75), the maximum stress was in the short vertical GFRP stirrups located in the lower chord below the opening. Figure 39 shows that the beam models DB-X0.50-Y0.0.33 and DB-X0.50-Y0.75 exhibited a maximum stress in the vertical GFRP stirrups of 375 and 315 MPa, respectively, which was typically located in the full-depth vertical stirrup at one of the sides of the opening. The maximum GFRP stress in model DB-X0.50-Y0.50 (477 MPa) was in the two full-depth vertical stirrups located at both sides of the opening. For the beam models with x_o/X_c = 0.75 (Figure 40), the maximum stress in the vertical GFRP stirrups ranged from 333 to 452 MPa. The top horizontal part of the vertical stirrup below the load point in DB-X0.75-Y0.33 reached 98% of the tensile strength of the bent portion of the GFRP. The maximum GFRP stress for the beam model DB-X0.75-Y0.50 was in one of the short GFRP stirrups in the top chord above the opening and in the full-depth vertical GFRP stirrup at the side of the opening closer to the support. For the beam model DB-X0.75-Y0.75, the maximum stress was in the full-depth vertical GFRP stirrup at the side of the opening closer to the support.

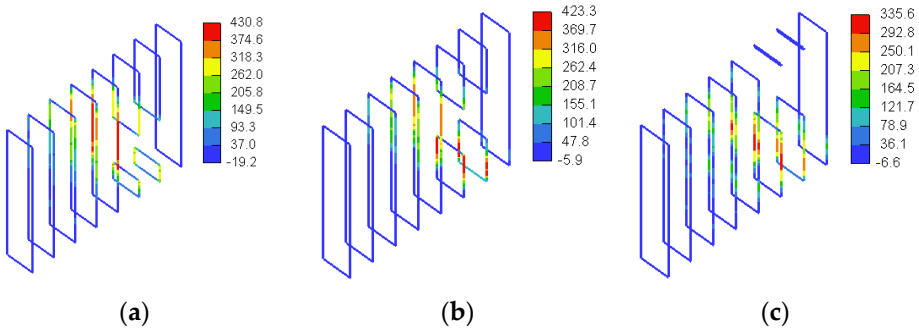

Figure 38. Three-dimensional view of stresses in GFRP bars for models with x_o/X_c = 0.25 (MPa): (**a**) DB-X0.25-Y0.33; (**b**) DB-X0.25-Y0.50; (**c**) DB-X0.25-Y0.75.

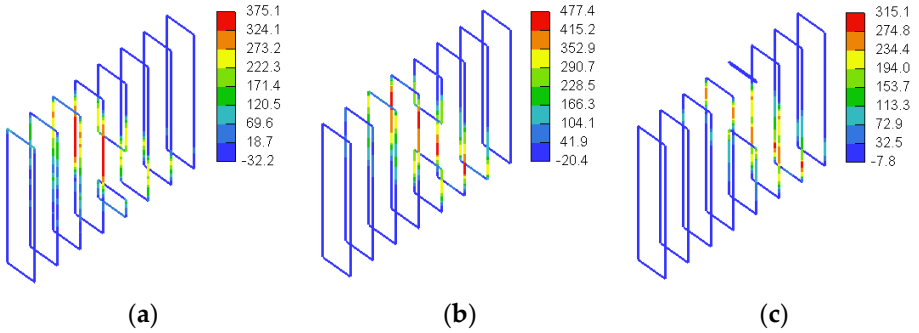

Figure 39. Three-dimensional view of stresses in GFRP bars for models with x_o/X_c = 0.50 (MPa): (**a**) DB-X0.50-Y0.33; (**b**) DB-X0.50-Y0.50; (**c**) DB-X0.50-Y0.75.

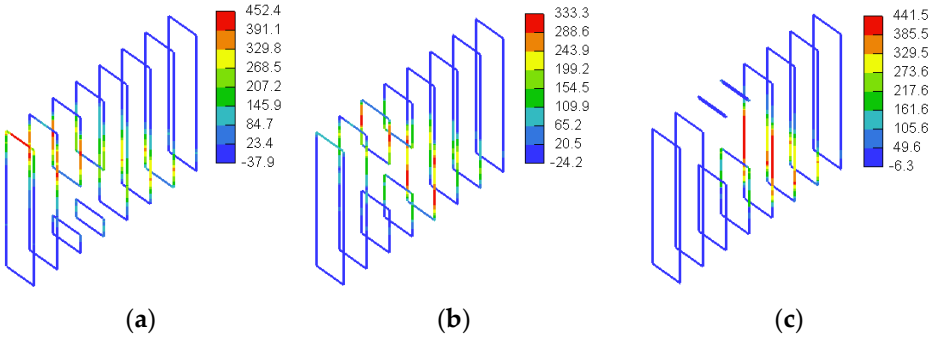

Figure 40. Three-dimensional view of stresses in GFRP bars for models with x_o/X_c = 0.75 (MPa): (**a**) DB-X0.75-Y0.33; (**b**) DB-X0.75-Y0.50; (**c**) DB-X0.75-Y0.75.

Figures 41–46 show stresses in the horizontal web reinforcement and tensile flexural reinforcement predicted numerically for the beam models of this group. None of the horizontal web reinforcing bars or the flexural reinforcement at the tension side in the deep beam models of this group reached their tensile strength. Generally, the maximum stress in the horizontal GFRP bars was on average 275 MPa (23% of the tensile strength of straight GFRP bars), with a minimum of 188 MPa (16% of the tensile strength of straight GFRP bars) and a maximum of 325 MPa (27% of the tensile strength of straight GFRP bars). The stresses in the flexural tensile GFRP reinforcement within the shear span were almost constant, except at the region near the support which exhibited reduced values of GFRP stresses. The near-uniform stress distribution of the GFRP stress in the flexural GFRP reinforcing bars within the shear span indicated that they acted as a tie, which is in alignment with the behavior of D-regions. The maximum stress in the flexural GFRP bars was on average 240 MPa (24% of the tensile strength of straight GFRP bars), with a minimum of 176 MPa (18% of the tensile strength of straight GFRP bars) and a maximum of 386 MPa (39% of the tensile strength of straight GFRP bars). The value of the maximum GFRP stress was dependent on the value of the ultimate load. The beam models with the higher ultimate load typically exhibited higher GFRP stresses in the flexural reinforcement at peak load. For instance, the smallest longitudinal GFRP stresses of 176, 184, and 190 MPa were recorded for the beam models DB-X0.25-Y0.50, DB-X0.50-Y0.75, and DB-X0.75-Y0.75 having the lowest ultimate loads. The greatest longitudinal GFRP stress of 386 MPa was recorded for the beam model DB-0.75-0.33 having the greatest ultimate load.

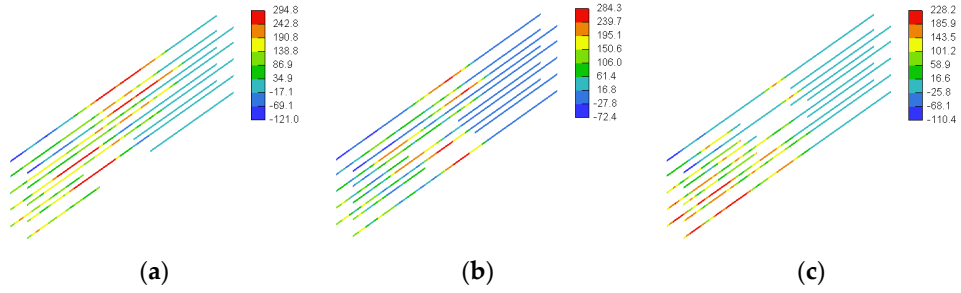

Figure 41. Stresses in horizontal GFRP web reinforcement for models with x_o/X_c = 0.25 (MPa): (**a**) DB-X0.25-Y0.33; (**b**) DB-X0.25-Y0.50; (**c**) DB-X0.25-Y0.75.

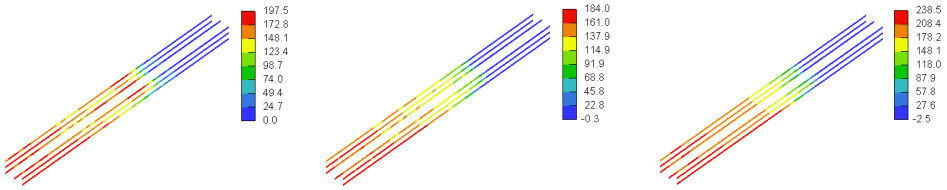

(**a**) (**b**) (**c**)

Figure 42. Stresses in bottom GFRP flexural reinforcement for models with x_o/X_c = 0.25 (MPa): (**a**) DB-X0.25-Y0.33; (**b**) DB-X0.25-Y0.50; (**c**) DB-X0.25-Y0.75.

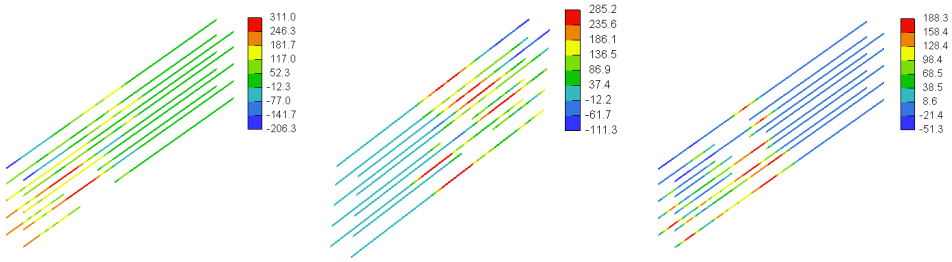

(**a**) (**b**) (**c**)

Figure 43. Stresses in horizontal GFRP web reinforcement for models with x_o/X_c = 0.50 (MPa): (**a**) DB-X0.50-Y0.33; (**b**) DB-X0.50-Y0.50; (**c**) DB-X0.50-Y0.75.

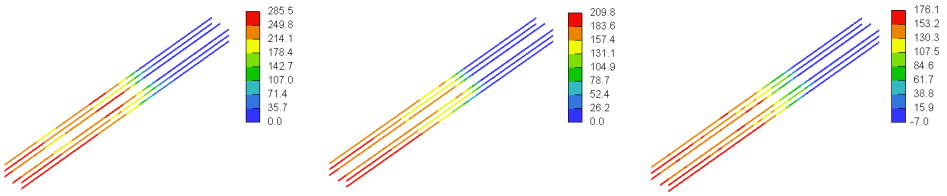

(**a**) (**b**) (**c**)

Figure 44. Stresses in bottom GFRP flexural reinforcement for models with x_o/X_c = 0.50 (MPa): (**a**) DB-X0.50-Y0.33; (**b**) DB-X0.50-Y0.50; (**c**) DB-X0.50-Y0.75.

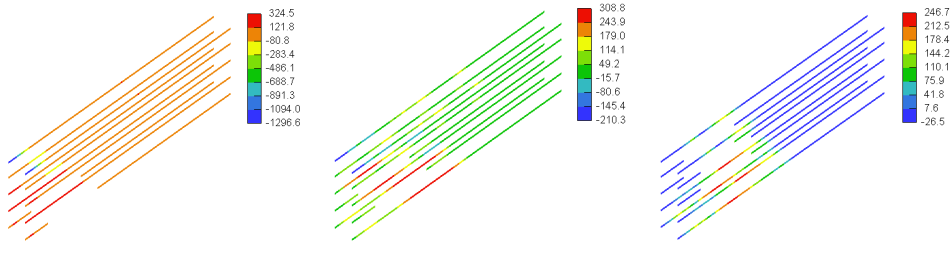

(**a**) (**b**) (**c**)

Figure 45. Stresses in horizontal GFRP web reinforcement for models with x_o/X_c = 0.75 (MPa): (**a**) DB-X0.75-Y0.33; (**b**) DB-X0.75-Y0.50; (**c**) DB-X0.75-Y0.75.

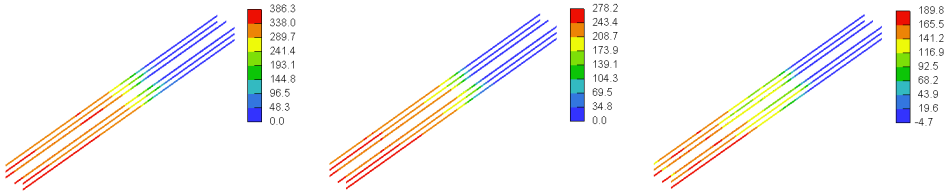

(**a**) (**b**) (**c**)

Figure 46. Stresses in bottom GFRP flexural reinforcement for models with x_o/X_c = 0.75 (MPa): (**a**) DB-X0.75-Y0.33; (**b**) DB-X0.75-Y0.50; (**c**) DB-X0.75-Y0.75.

5. Simplified Analytical Formulas

5.1. Deep Beam Models with Different Opening Locations

Kong and Sharp [38] developed Equation (1) to determine the ultimate shear strength (V_u) of steel-reinforced deep beams with a web opening, noting that the ultimate load (P_u) of the deep beams of the present study equals $2V_u$. In these equations, X_c = clear shear span, f_t = tensile strength of the concrete, b = width of the beam, h = total depth of the beam, A = area of an individual web bar or a main reinforcing bar, y_1 = depth at which a typical bar intersects a potential critical shear crack, α_1 = angle of inclination between a typical bar and the critical shear crack, C_1 = 1.4 for normal weight concrete, and C_2 = 300 N/mm^2 for deformed steel bars. The coefficients $a_1 = w_o/2X_c$ and $a_2 = h_o/2h$ define the opening size. The coefficients $K_1 = X_o/X_c$ and $K_2 = Y_o/h$ define the position of the opening, where X_o = horizontal distance between the center of the opening and the inner face of the support plate and Y_o = vertical distance between the center of the opening and the bottom face of the beam. The coefficient λ = 1.0 for the main longitudinal bars, whereas for web reinforcing bars, λ = 1.5. Table 7 compares predictions of Kong's Equation (1) [38] for the GFRP-reinforced deep beams with a web opening in the middle of the shear span included in the parametric study to the strengths predicted by the numerical analysis. It is evident that Kong's Equation (1) consistently overestimated the ultimate loads of the deep beam models with a web opening in the middle of the shear span by up to 20%. The unconservative predictions provided by Kong's Equation (1) [38] could be attributed to the reduced dowel action and Young's modulus of the GFRP longitudinal reinforcement. As such, Equation (2) is proposed in the present study to represent a refined formula to estimate V_u of GFRP-reinforced concrete deep beams with a web opening in the middle of the shear span, where A_f = individual area of a main reinforcing bar, A_w = individual area of a web reinforcing bar, E_f = elastic modulus of the main GFRP reinforcing bars (66.4 GPa), and E_s = elastic modulus of steel bars (200 GPa). As shown in Table 7, predictions of the refined analytical formula provided a conservative prediction for the ultimate loads of the deep beam models with an opening in the middle of the shear span.

$$V_u = C_1\left[1 - 0.35\frac{(K_1+a_1)X_c}{(K_2-a_2)h}\right] f_t b(K_2-a_2)h + \sum \lambda C_2 A \frac{y_1}{h}\sin^2\alpha_1 \quad (1)$$

$$V_u = C_1\left[1 - 0.35\frac{(K_1+a_1)X_c}{(K_2-a_2)h}\right] f_t b(K_2-a_2)h + \sum C_2 \frac{E_f}{E_s} A_f \frac{y_1}{h}\sin^2\alpha_1 + \sum \lambda C_2 A_w \frac{y_1}{h}\sin^2\alpha_1 \quad (2)$$

Table 7. Comparison between predictions of the analytical formulas and numerical results of deep beams with an opening in the middle of the shear span.

Model	Ultimate Load (kN)				
	Numerical	Kong's Formula [38] Equation (1)		Refined Formula Equation (2)	
		Prediction	Error (%) [1]	Prediction	Error (%) [1]
DB-W0.16-H0.17	1789	1942	+9	1378	−23
DB-W0.16-H0.25	1637	1863	+14	1373	−16
DB-W0.16-H0.33	1327	1385	+4	966	−27
DB-W0.27-H0.17	1678	1928	+15	1438	−14
DB-W0.27-H0.25	1504	1709	+14	1291	−14
DB-W0.27-H0.33	1239	1242	+1	892	−28
DB-W0.32-H0.17	1585	1871	+18	1405	−11
DB-W0.32-H0.25	1374	1653	+20	1258	−8
DB-W0.32-H0.33	1019	1038	+2	709	−30

[1] Error (%) $= \frac{\text{Formula}-\text{Numerical}}{\text{Numerical}} \times 100$.

5.2. Deep Beams with a Web Opening Shifted from the Midpoint of the Shear Span

Table 8 compares predictions of Kong's Equation (1) [38] for the GFRP-reinforced deep beams with a web opening at different locations within the shear span. It is evident that Kong's Equation (1) [38] provided inconsistent results. In many cases, the prediction of Equation (1) was significantly higher than the strength obtained from the numerical analysis. In some other cases, the prediction of Equation (1) was lower. It is noteworthy that Equation (2) proposed in the current study did not provide satisfactory results when the center of the web opening was shifted from the middle of the shear span. These results indicate that for GFRP-reinforced beams with a web opening shifted from the middle of the shear span, a modified Equation should be adopted. As such, the refined formula given in Equation (3) is proposed for the prediction of the shear strength of GFRP-reinforced deep beams with a web opening shifted from the midpoint of the shear span. Two coefficients were introduced in this formula, namely λ_1 and λ_2, to account for the opening size and location, respectively. These two coefficients were proposed based on careful examination of the ultimate loads of the deep beam models with a web opening shifted from the middle of the shear span. The results of the parametric study showed an increase in the ultimate load with an increase in the distance from the support for the beam models with K_2 values of 0.33 and 0.5. The results of the parametric study also indicated that when the center of the opening was located at a K_2 value of 0.75, a reduction in the ultimate load was recorded with an increase in the distance from the support. The coefficient λ_2 reflects the trend of the results of the parametric study. The predictions of Equation (3) are in good agreement with the results of the numerical analysis. It is noteworthy that Equation (3) also provided reasonable predictions (deviation $\leq$ 12%) for the shear strength of the GFRP-reinforced concrete deep beams with an opening in the middle of the shear span having $h_o/h \leq 0.25$.

$$V_u = \lambda_1 \lambda_2 C_1 \left[1 - 0.35\frac{X_c}{h}\right] f_t bh + \sum C_2 \frac{E_f}{E_s} A_f \frac{y_1}{h} \sin^2 \alpha_1 + \sum C_2 A_w \frac{y_1}{h} \sin^2 \alpha_1 \quad (3)$$

$$\lambda_1 = (1 - a_1)(1 - a_2)$$

$$\lambda_2 = \left[1 - \frac{K_2}{3K_1}\right]; \text{ when } K_2 = 0.33 \text{ or } 0.50$$

$$\lambda_2 = \left[1 - \frac{K_1}{1.15K_2}\right]; \text{ when } K_2 = 0.75$$

Table 8. Comparing predictions of the analytical formulas and numerical results of deep beams with an opening shifted from the midpoint of the shear span.

Model	Ultimate Load (kN)				
	Numerical	Kong's Formula [38] Equation (1)		Refined Formula Equation (3)	
		Prediction	Error (%) [1]	Prediction	Error (%) [1]
DB-X0.25-Y0.33	1478	1216	−18	1436	−3
DB-X0.25-Y0.50	1337	2264	+69	1188	−11
DB-X0.25-Y0.75	1714	3513	+105	1848	8
DB-X0.50-Y0.33	1971	916	−54	1825	−7
DB-X0.50-Y0.50	1504	1709	+14	1683	12
DB-X0.50-Y0.75	1259	2863	+127	1349	7
DB-X0.75-Y0.33	2429	1042	−57	2055	−15
DB-X0.75-Y0.50	1884	1461	−22	1877	0
DB-X0.75-Y0.75	1139	2399	+111	910	−20

[1] Error (%) $= \frac{\text{Formula} - \text{Numerical}}{\text{Numerical}} \times 100$.

6. Conclusions

This study provided new knowledge on the structural behavior of GFRP-reinforced concrete deep beams with a web opening through a numerical analysis. The simulation models developed in the current study served as a numerical platform for performance prediction of GFRP-reinforced deep beams with a web opening. The size and location of the web opening within the shear span played a primary role in the behavior of the deep beam models. Placing a web opening in the compression zone close to the support or the load plate was very detrimental to the beam strength. In contrast, a negligible strength reduction was recorded when the web opening was placed in the tension side above the flexural reinforcement and away from the natural load path and the support plate. Specific conclusions of the work are summarized below.

- For the beam models with y_o/h values of 0.33 and 0.50, the strength increased with an increase in the distance measured from the face of the support within the shear span. The strength of the beam models with a y_o/h of 0.33 tended to be higher than that of their counterparts with a y_o/h of 0.50, and this behavior was more evident with an increase in the distance from the face of the support plate. The beam models with a y_o/h of 0.75 exhibited an opposite trend, where the strength decreased with an increase in the distance measured from the face of the support within the shear span because such a movement resulted in an opening closer the load plate.
- For the beam models having a web opening closer to the support plate (x_o/X_c = 0.25), strength reductions of 43 and 49% were recorded at y_o/h values of 0.33 and 0.50, respectively. When the opening was pushed upward away from the natural load path (x_o/X_c = 0.25 and y_o/h = 0.75), a lower strength reduction of 34% was recorded.
- For the beam models having a web opening with an x_o/X_c of 0.50, strength reductions of 24, 42, and 52% were recorded at y_o/h values of 0.33, 0.50, and 0.75, respectively.
- The beam model with x_o/X_c = 0.75 and y_o/h = 0.33 exhibited a negligible strength reduction of 7% because the web opening was in the tension side and did not interrupt the natural load path. In contrast, the beam model with a web opening closer to the load plate (x_o/X_c = 0.75 and y_o/h = 0.75) exhibited a significant strength reduction of 56% because the web opening was in the compression zone close to the load plate and fully interrupted the natural load path.
- For the beam models with a web opening in the middle of the shear span, the strength decreased with an increase in either the opening width or height. The rate of the strength reduction caused by increasing the opening height was, however, more significant than that produced by increasing the opening width. At the same w_o/a of 0.16, strength reductions of 31–49% were recorded for the deep beam models having an opening in the midpoint of the shear span with h_o/h values of 0.17–0.33. More pronounced respective strength reductions of 39–61% were recorded for the deep beam models with the greater w_o/a of 0.32.
- The existing empirical equation for concrete deep beams reinforced with conventional steel bars with a web opening provided unconservative and/or inconsistent predictions for the ultimate load of the beam models reinforced with GFRP bars.
- Refined empirical equations were introduced for shear strength prediction of GFRP-reinforced concrete deep beams with a web opening of different sizes and locations within the shear span. The refined analytical formulas tended to provide conservative/reasonable predictions for the shear capacity of the GFRP-reinforced concrete deep beams considered in the present study.
- The simulation models developed and verified in the present study can be used as a numerical platform in future research to study the effect of using different types of reinforcing bars (e.g., carbon, glass, steel with different yield strengths) on the behavior of concrete deep beams with and without a web opening in the shear span. Future research should further investigate the effect of the anchorage length and bond condition of GFRP reinforcing bars on the response of the GFRP-reinforced deep beams.

Author Contributions: Conceptualization, T.E.-M. and N.K.; methodology, A.S.-S., T.E.-M. and N.K.; software, A.S.-S. and N.K.; validation, A.S.-S., T.E.-M. and N.K.; formal analysis, A.S.-S., T.E.-M. and N.K.; investigation, A.S.-S., T.E.-M. and N.K.; resources, T.E.-M.; data curation, A.S.-S.; writing—original draft preparation, A.S.-S., T.E.-M. and N.K.; writing—review and editing, A.S.-S., T.E.-M. and N.K.; visualization, A.S.-S.; supervision, T.E.-M. and N.K.; project administration, T.E.-M.; funding acquisition, T.E.-M. All authors have read and agreed to the published version of the manuscript.

Funding: This project is supported by the United Arab Emirates University (UAEU) [grant number 12N172].

Data Availability Statement: The data presented in this study are available on request from the corresponding author. The data are not publicly available due to privacy issues.

Conflicts of Interest: The authors declare no conflicts of interest.

References

1. American Concrete Institute ACI. *Building Code Requirements for Structural Concrete and Commentary on Building Code Requirements for Structural Concrete (ACI 318R-19)*; American Concrete Institute (ACI): Farmington Hills, MI, USA, 2014.
2. MacGregor, J.; Wight, J. *Reinforced Concrete Mechanics and Design*, 4th ed.; SI Units; Prentice Hall: Singapore, 2005.
3. Kong, F. *Reinforced Concrete Deep Beams*; Blackie and Son Ltd.: London, UK, 1999.
4. Mansour, M.; Tan, K.-H. *Concrete Beams with Openings Analysis and Design*; CRC Press: New York, NY, USA, 1999.
5. *CSA S806-12*; Design and Construction of Building Structures with Fiber-Reinforced Polymers. Canadian Standards Association CSA: Mississauga, ON, Canada, 2012.
6. *ACI 440.1R-15*; ACI Committee 440. Guide for the Design and Construction of Structural Concrete Reinforced with Fiber-Reinforced Polymer (FRP) Bars. American Concrete Institute (ACI): Farmington Hills, MI, USA, 2019.
7. Bakis, C.; Bank, L.; Brown, V.; Cosenza, E.; Davalos, J.; Lesko, J.; Machida, A.; Rizkalla, S.; Triantafillou, T. Fiber-reinforced polymer composites for construction-state-of-the-art review. *J. Compos. Constr.* **2002**, *6*, 73–87. [CrossRef]
8. Bank, L. *Composites for Construction: Structural Design with FRP Materials*; John Wiley & Sons: Hoboken, NJ, USA, 2006.
9. Gangarao, H.; Taly, N.; Vijay, P. *Reinforced Concrete Design with FRP Composites*; CRC Press: New York, NY, USA, 2006.
10. Nanni, A.; De Luca, A.; Zadeh, H. *Reinforced Concrete with FRP Bars: Mechanics and Design*; CRC Press: New York, NY, USA, 2014.
11. Omeman, Z.; Nehdi, M.; El-Chabib, H. Experimental study on shear behavior of carbon fiber-reinforced polymer reinforced concrete short beams without web reinforcement. *Can. J. Civ. Eng.* **2008**, *35*, 1–10. [CrossRef]
12. Abed, F.; El-Chabib, H.; Alhamaydeh, M. Shear characteristics of GFRP reinforced polymer reinforced concrete deep beams without web reinforcement. *J. Reinf. Plast. Compos.* **2012**, *31*, 1063–1073. [CrossRef]
13. Farghaly, A.S.; Benmokrane, B. Shear behavior of FRP-reinforced concrete deep beams without web reinforcement. *J. Compos. Constr.* **2013**, *17*, 04013015. [CrossRef]
14. Andermatt, M.; Lubell, A. Behavior of concrete deep beams reinforced with internal fiber-reinforced polymer—Experimental study. *ACI Struct. J.* **2013**, *110*, 585–594.
15. Kim, D.; Lee, j.; Lee, Y. Effectiveness factor of strut-and-tie model for concrete deep beams reinforced with FRP rebars. *Compos. Part B* **2014**, *56*, 117–125. [CrossRef]
16. Liu, H.; Yang, J.; Wang, X.; Han, D. Experimental study on shear behavior of BFRP-reinforced recycled aggregate concrete deep beams without stirrups. KSCE. *J. Civ. Eng.* **2016**, *21*, 2289–2299.
17. Alhamad, S.; Al-Banna, Y.; Al-Osman, A.; Mouthassseeb, J.; Abdalla, S.; Abed, F. Effect of shear span-to-depth ratio on the shear behavior of BFRP-RC deep beams. *MATEC* **2017**, *120*, 01012. [CrossRef]
18. Abed, F.; El-Refai, A.; Abdalla, S. Experimental and finite element investigation of the shear performance of BFRP-RC short beams. *Structures* **2019**, *20*, 689–701. [CrossRef]
19. Abu-Obaida, A.; El-Ariss, B.; El-Maaddawy, T. Behavior of short-span concrete members internally reinforced with glass fiber–reinforced polymer bars. *J. Compos. Constr.* **2018**, *22*, 04018038. [CrossRef]
20. Syroka-Korol, E.; Tejchman, J.; Mroz, Z. Experimental and numerical assessment of size effect in geometrically similar slender concrete beams with basalt reinforcement. *Eng. Struct.* **2017**, *141*, 272–291. [CrossRef]
21. Mohamed, K.; Farghaly, A.S.; Benmokrane, B. Effect of vertical and horizontal web reinforcement on the strength and deformation of concrete deep beams reinforced with GFRP bars. *J. Struct. Eng.* **2017**, *143*, 04017079. [CrossRef]
22. Song, B.; Jin, L.; Zhang, J.; Du, X. Size effect tests on shear strength of Basalt FRP-RC deep beams with different shear-span ratios. *Eng. Struct.* **2023**, *294*, 116740. [CrossRef]
23. Frappier, J.; Mohamed, K.; Farghaly, A.; Benmokrane, B. Behavior and strength of glass fiber-reinforced polymer reinforced concrete deep beams with web openings. *ACI Struct. J.* **2019**, *116*, 275–285. [CrossRef]
24. Arabasi, S.; El-Maaddawy, T. Reinforcing of discontinuity regions in concrete deep beams with GFRP composite bars. *Compos. Part C Open Access* **2020**, *3*, 100064. [CrossRef]

25. Ge, W.; Zhang, J.; Cao, D.; Tu, Y. Flexural behaviors of hybrid concrete beams reinforced with BFRP bars and steel bars. *Constr. Build. Mater.* **2015**, *87*, 28–37. [CrossRef]
26. Kazemi, M.; Daneshfar, M.; Zandi, Y.; Agdas, A.S.; Yousefieh, N.; Mohammadifar, L.; Rahmani, A.; Saberian, M.; Mamdouh, A.; Khadimallah, M.A.; et al. Effects of the Concrete Strength and FRP Reinforcement Type on the Non-Linear Behavior of Concrete Deep Beams. *Sustainability* **2022**, *14*, 4136. [CrossRef]
27. Brown, M.; Bayrak, O. Investigation of deep beams with various load configurations. *ACI Struct. J.* **2007**, *104*, 611–620.
28. Tan, K.; Lu, H. Shear behavior of large reinforced concrete deep beams and code comparison. *ACI Struct. J.* **1999**, *96*, 836–845.
29. Mihaylov, B.; Bentz, E.; Collins, M. Behavior of large deep beams subjected to monotonic and reversed cyclic shear. *ACI Struct. J.* **2010**, *107*, 726–734.
30. Sheikh-Sobeh, A. Numerical Simulation of Concrete Beams with Discontinuity Regions Reinforced with Nonmetallic Reinforcing Bars. Master's Thesis, United Arab Emirates University, Abu Dhabi, United Arab Emirates, June 2023.
31. ATENA Computer Software, Cervenka Consulting s.r.o.: Prague, Czech Republic. Available online: https://www.cervenka.cz/ (accessed on 25 March 2022).
32. Imjai, T.; Guadagnini, M.; Pilakoutas, K. Bend strength of FRP bars: Experimental investigation and bond modeling. *J. Mater. Civ. Eng.* **2017**, *29*, 04017024. [CrossRef]
33. Imjai, T.; Garcia, R.; Guadagnini, M.; Pilakoutas, K. Strength degradation in curved fiber-reinforced polymer (FRP) bars used as concrete reinforcement. *Polymers* **2020**, *12*, 1653. [CrossRef] [PubMed]
34. Gooranorimi, O.; Claure, G.; Suaris, W.; Nanni, A. Bond-slip effect in flexural behavior of GFRP RC slabs. *Compos. Struct.* **2018**, *193*, 80–86. [CrossRef]
35. Sheikh-Sobeh, A.; Kachouh, N.; El-Maaddawy, T. Numerical analysis of concrete deep beams reinforced with glass fiber-reinforced polymer bars. *Buildings* **2023**, *13*, 2767. [CrossRef]
36. Yang, K.; Eun, H.; Chung, H. The influence of web openings on the structural behavior of reinforced high-strength concrete deep beams. *Eng. Struct.* **2006**, *28*, 1825–1834. [CrossRef]
37. El-Maaddawy, T.; El-Ariss, B. Behavior of concrete beams with short shear span and web opening strengthened in shear with CFRP composites. *J. Compos. Constr.* **2012**, *16*, 47–59. [CrossRef]
38. Kong, F.; Sharp, G. Structural idealisation for deep beams with web openings. *Mag. Concr. Res.* **1977**, *29*, 81–91. [CrossRef]